

# 博士學位論文

Developments of quantitative and non-invasive methods  
for evaluating mechanical property of the knee articular  
cartilage

膝関節軟骨力学特性の非侵襲的定量的評価法に関する研究

平成 25 年 1 月 10 日 提出

首都大学東京 大学院

人間健康科学研究科 博士後期課程 人間健康科学専攻

放射線科学域

学修番号：10997601

氏 名：青木 孝子

(指導教員名： 古川 顕 教授)

# 博 士 学 位 論 文

Developments of quantitative and non-invasive methods for  
evaluating mechanical property of the knee articular cartilage

膝関節軟骨力学特性の非侵襲的定量的評価法に関する研究

平成 25 年 1 月 10 日 提出

首都大学東京 大学院

人間健康科学研究科 博士後期課程 人間健康科学専攻

放射線科学域

学修番号：10997601

氏 名：青木 孝子

(指導教員名： 古川 顕 教授)

## Contents

<b>Overview</b> .....	1
<b>Chapter 1</b> prolegomenon.....	2
1.1 Background.....	2
1.2 Objective.....	2
1.3 Contribution.....	3
1.4 Approach.....	3
1.5 Constitution .....	3
1.6 Conflict of interest.....	4
<b>Chapter 2</b> Mechanism of osteoarthritis and cartilaginous relations.....	5
2.1 Cartilaginous structure.....	5
2.2 Change of the articular cartilage with osteoarthritis.....	8
2.3 Evaluation of OA.....	10
2.3.1 Initial consultation .....	11
2.3.2 Kellgren-Lawrence Score .....	11
2.3.3 Outerbridge classification.....	12
2.3.4 Modified Outerbridge classification using MRI.....	13
2.3.5 Quantitative cartilage imaging using MRI .....	14
<b>Chapter 3</b> Microscopic water molecule motion in the cartilage obtained from diffusion weighted images.....	16
3.1 Free diffusion.....	16
3.2 Restricted diffusion.....	19
3.3 Diffusion in articular cartilage.....	21
<b>Chapter 4</b> Evaluating relation between apparent diffusion coefficient and viscoelasticity of the cartilage .....	25
4.1 Introduction .....	25
4.2 Theory supported T1p.....	27
4.2.1 Spin-Lock pulse.....	27
4.2.2 Magnetization in the rotating frame .....	28
4.2.3 T1p-prepared segmented multi-shot 3D-TFE sequence .....	30
4.2.4 Behavior of the magnetization of the transient period .....	32
4.2.5 Artifact.....	33
4.3 Basic points of mechanical property .....	34
4.3.1 Viscoelasticity .....	34
4.3.2 Effect of temperature on viscoelastic behavior .....	35

4.3.3 Stress relaxation.....	35
4.4 Material and Methods.....	37
4.4.1 Subjects.....	37
4.4.2 MR Imaging.....	37
4.4.3 ROI setting.....	39
4.4.4 Mechanical testing.....	41
4.4.5 Statistical analysis .....	42
4.5 Results .....	43
4.6 Discussion.....	46
4.7 Conclusion.....	49
<b>Chapter 5</b> Evaluating relation between speed of sound and elasticity of the cartilage .....	50
5.1 Introduction .....	50
5.2 Theory supporting the speed of sound measurements.....	52
5.2.1 Basic ultrasound .....	52
5.2.2 Incidence angle and the distance .....	54
5.2.3 The transmission method measurement of speed of sound (SOS) .....	55
5.2.4 The SOS measurement by combination method .....	57
5.3 Materials and Methods .....	59
5.3.1 Specimen preparation .....	59
5.3.2 MRI imaging .....	60
5.3.3 Thickness measurements of specimens .....	61
5.3.4 SOS measurements in cartilage specimens .....	63
5.3.5 Statistics.....	64
5.4 Results .....	65
5.4.1 Thickness measurements of specimens .....	65
5.4.2 Comparison of SOS using transmission method and combination method ..	65
5.5 Discussion.....	67
5.6 Conclusions .....	69
<b>Chapter 6</b> Comparison of the speed of sound and T2 relaxation time of the cartilage in the assessment of its degenerative change.....	70
6.1 Introduction .....	70
6.2 Materials and Methods .....	71
6.2.1 Subjects.....	71
6.2.2 MR imaging.....	71
6.2.3 Problem of applying the pulse-echo method .....	72



6.2.4 Applying the real-time virtual sonography (RVS).....	74
6.2.5 Definition of the cartilage thickness.....	77
6.2.6 Statistics.....	78
6.3 Results .....	79
6.4 Discussion.....	80
6.5 Conclusions .....	83
<b>Chapter 7</b> Summery .....	84
<b>References</b> .....	87
Chapter 1 .....	87
Chapter 2 .....	88
Chapter 3 .....	89
Chapter 4 .....	90
Chapter 5 .....	96
Chapter 6 .....	99
<b>Acknowledgment</b> .....	103

## Overview

変形性膝関節症（OA）は加齢性に増加し、超高齢化社会において生活の質の維持や医療経済にとって深刻な疾患の一つである。近年、OA 初期の加療において進行の抑制が期待される抗 OA 薬が開発されたが、OA 初期の診断法は確立されていないため早期診断は困難で、整形外科受診時にはかなり進行している。軟骨は主に 70-80%の水分と細胞外基質で構成され、軟骨細胞はわずかで血管、神経、リンパ管はなく、膝の運動による関節液の流動により栄養され、細胞外基質であるコラーゲン線維とプロテオグリカンが軟骨機能の維持に重要な役割を担っている。軟骨表層のコラーゲン線維は関節面と並走し軟骨にかかる荷重を支え、プロテオグリカンは水分を保持しクッションの役割を担う。加齢とともにコラーゲンの変性とプロテオグリカンの減少が同時に進行していき、最終的に荷重を支えることができなくなり軟骨が破壊される。軟骨は修復・再生されることはないため、軟骨が変性し OA へ進行していくと、姑息的対症療法の後、最終的に骨切り術または人工関節置換術の手術適応となるが、高齢者では自立した生活は困難になる。従って、軟骨変性に伴う変化を定量評価することが OA 初期の診断に重要である。

本研究はコラーゲンの変性に伴う物理特性変化の定量的評価法を考案し、その測定精度を検証した。見かけの拡散係数（ADC）は含水量を示すとともに、吸水性を示すと考え、ブタ軟骨を用いて力学試験による粘弾性と ADC の高い相関を確認した。寒天ファントムを用いて基礎実験を行い、MRI と超音波を併用した軟骨の音速測定法の測定精度を確認した。MRI と超音波を併用した軟骨の音速測定法を生体へ応用し、ボランティア（倫理申請で承認され、同意の得られた者）による測定で T2 値と高い相関が得られた。音速は T2 と同じ現象をとらえていることが示され、信頼性が得られた。本研究は不可能とされていた生体軟骨の非侵襲的物理的特性（弾性、粘弾性）の測定が可能であることを示した。

# **Chapter 1   prolegomenon**

## **1.1 Background**

Osteoarthritis (OA) is a degenerative disease of cartilage that progresses slowly by erosive deterioration of articular cartilage, and develops most commonly in weight-bearing regions. Structural change of the collagen array and decrease in water content by decreased proteoglycan occur in early stage of OA, [1-3] and capacity of the load support causes decline of the elasticity by structural change of the collagen array and becomes more serious with progress of disease [4]. Since symptoms do not appear in the early stage of OA, it progresses without noticing the onset. Diagnosis in early stage and control of progressive OA are important issue in super-graying society.

## **1.2 Objective**

The aim of this study was to develop noninvasive in-vivo measuring methods for the changes in the cartilage. The all studies were approved by the institutional review board.

### 1.3 Contribution

Development of new noninvasive quantitative evaluation methods assessing mechanical property of the cartilage using MRI and/or ultrasound for early detection and correct diagnosis of OA.

### 1.4 Approach

Newly developed two non-invasive quantitative evaluation methods using MRI and/or ultrasound to assess the mechanical property of the cartilage are demonstrated and their accuracies are discussed.

### 1.5 Constitution

In Chapter 2, describes basics point of OA. In Chapter 3 describes basics point of behavior of molecules diffusion. From Chapter 4 to 9, examines newly proposed method for assessing the elasticity, and summarizes this article in last chapter 10.



## 1.6 Conflict of interest

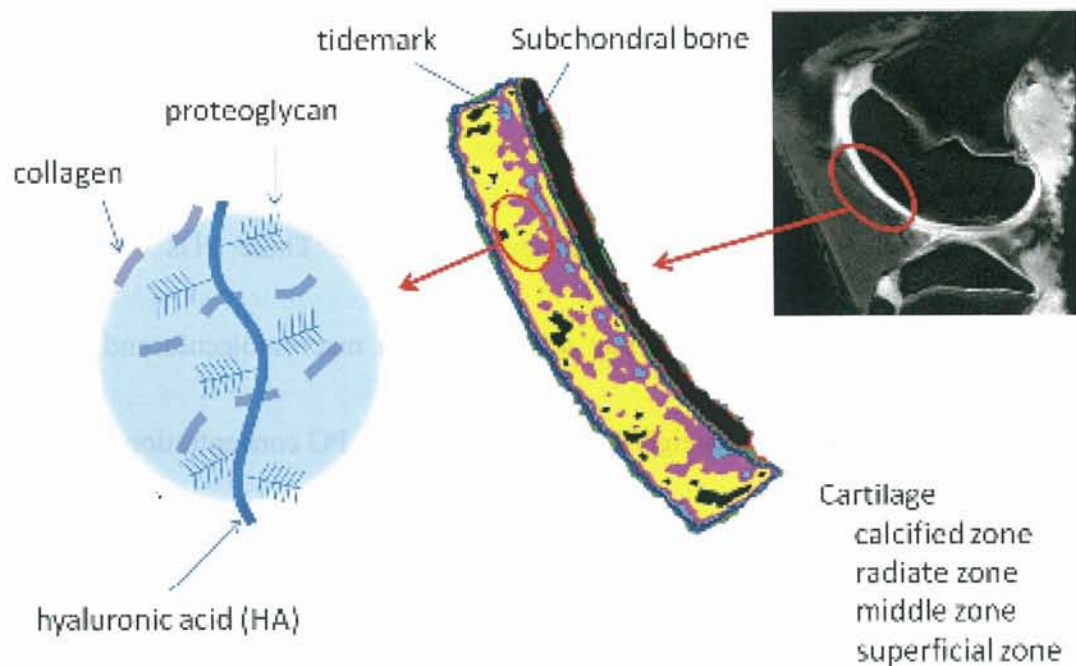
This reserch was conducted by a grant from Polcy-based medical services foundation.

## Chapter 2 Mechanism of osteoarthritis and cartilaginous relations

### 2.1 Cartilaginous structure

Articular cartilage is a living material composed of a relatively small number of cells known as chondrocytes surrounded by a multicomponent matrix. Approximately 70 to 85% weight of the whole tissue is water and the remainder of the tissue is composed primarily of proteoglycans (PG) and collagen (**Fig. 2-1**). These PGs can bind or aggregate to a backbone of hyaluronic acid to form a macromolecule and account approximately 30% of the dry weight of articular cartilage. PG concentration and water content vary through the depth of the tissue. Near the articular surface, PG concentration is relatively low and the water content is highest in the tissue. In the deeper regions of the cartilage, near subchondral bone, the PG concentration is greatest and the water content is lowest. Collagen is a fibrous protein that makes up 60 to 70% of the dry weight of the tissue. Type II is the predominant collagen in articular cartilage, although other types are present in smaller amounts. Collagen architecture varies through the depth of the tissue and the structure of articular cartilage is often

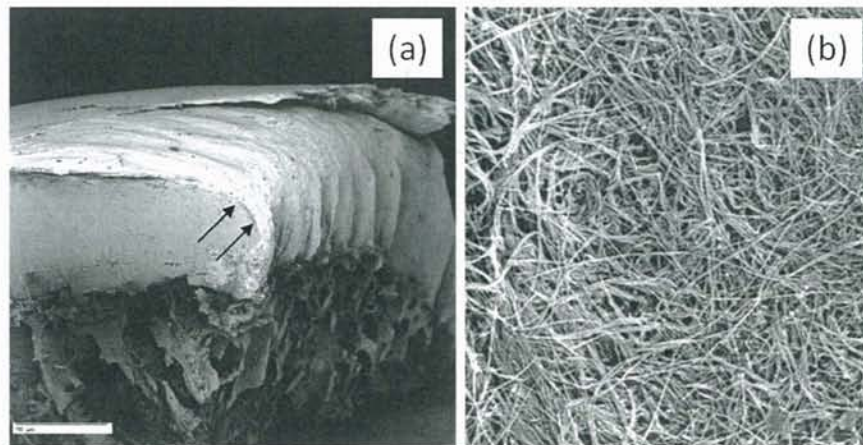
described in terms of four zones between the articular surface and the subchondral bone: the surface or superficial tangential zone, the intermediate or middle zone, the deep or radiate zone, and the calcified zone. The calcified cartilage is the boundary between the cartilage and the underlying subchondral bone. The interface between the deep zone and calcified cartilage is known as the tidemark [1].



**Fig. 2-1.** Schematic illustration of cartilaginous constitution

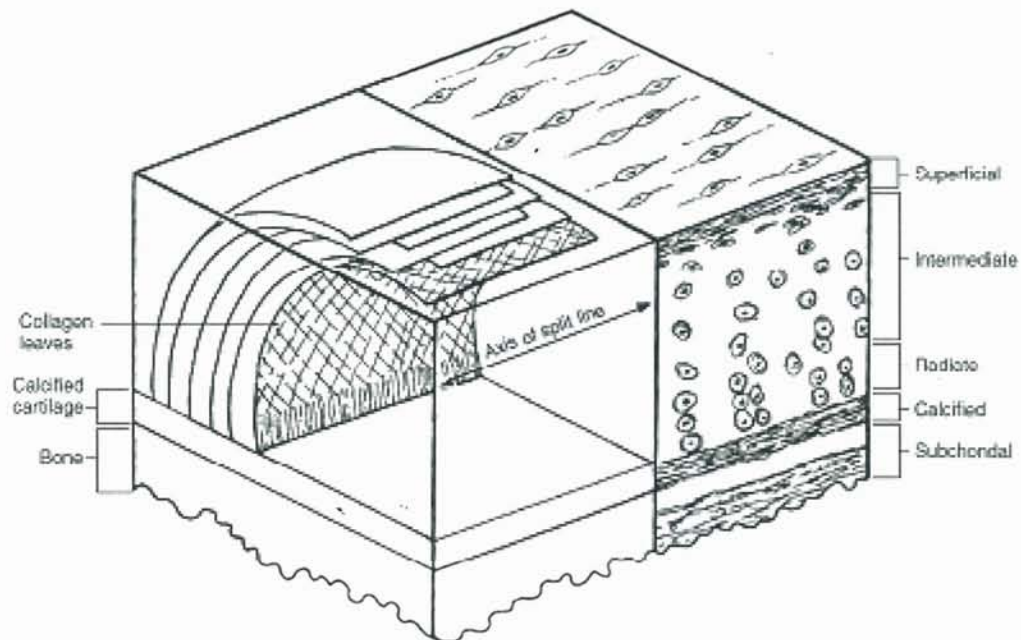
**Fig. 2-2** showed electron microscopy image of cartilage and high-power scanning electron microscopy image of deep layer. Matrix collagen within cartilage is organized in leaflike structures that radiate from the subchondral interface in a perpendicular

orientation and then curve into the horizontal orientation at the articular surface (**Fig. 2-3**).



**Fig. 2-2** Microstructure of cartilage

Electron microscopy image of cartilage (a) and high power electron microscopy image of the collagen network in deep layer (Radiate zone) (b). [2].



**Fig. 2-3** Collagen network orientation of cartilage [1]

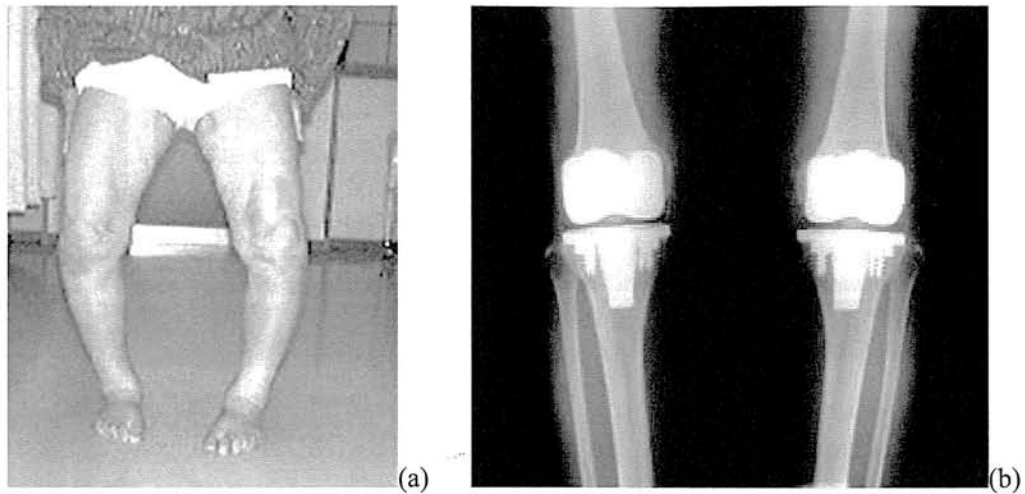


## 2.2 Change of the articular cartilage with osteoarthritis

Osteoarthritis is classified as primary when aetiology and pathogenesis are unknown.

The known causes are mechanical or metabolic risk factors such as aberrance of the axis, haemophilia, rheumatoid and bacterial arthritis, osteochondrosis dissecans, dysplasia of the joint, injury, etc. The most common joints involved in OA are the knee joints major risks come from occupations that require repetitive bending of the joint. Obesity may be a further factor in the development of osteoarthritis, particularly of the knee and especially in women. However, once osteoarthritis has developed, the work-related repetitive movement often makes the disorder worse [3].

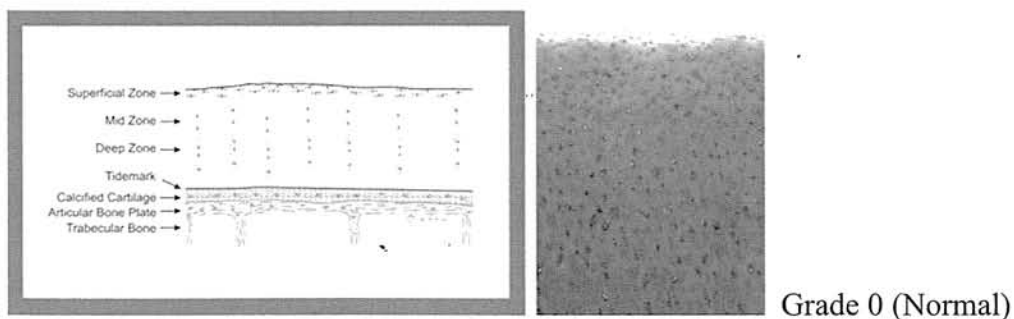
Since a self-repair function is poor and neither the nerve nor the blood vessel exists in cartilage, symptoms seldom occur in the early stage of the OA as the disease progress symptoms and deformity of the bones appear, and total knee replacement (TKR) is required at the terminal stage (**Fig. 2-4**).

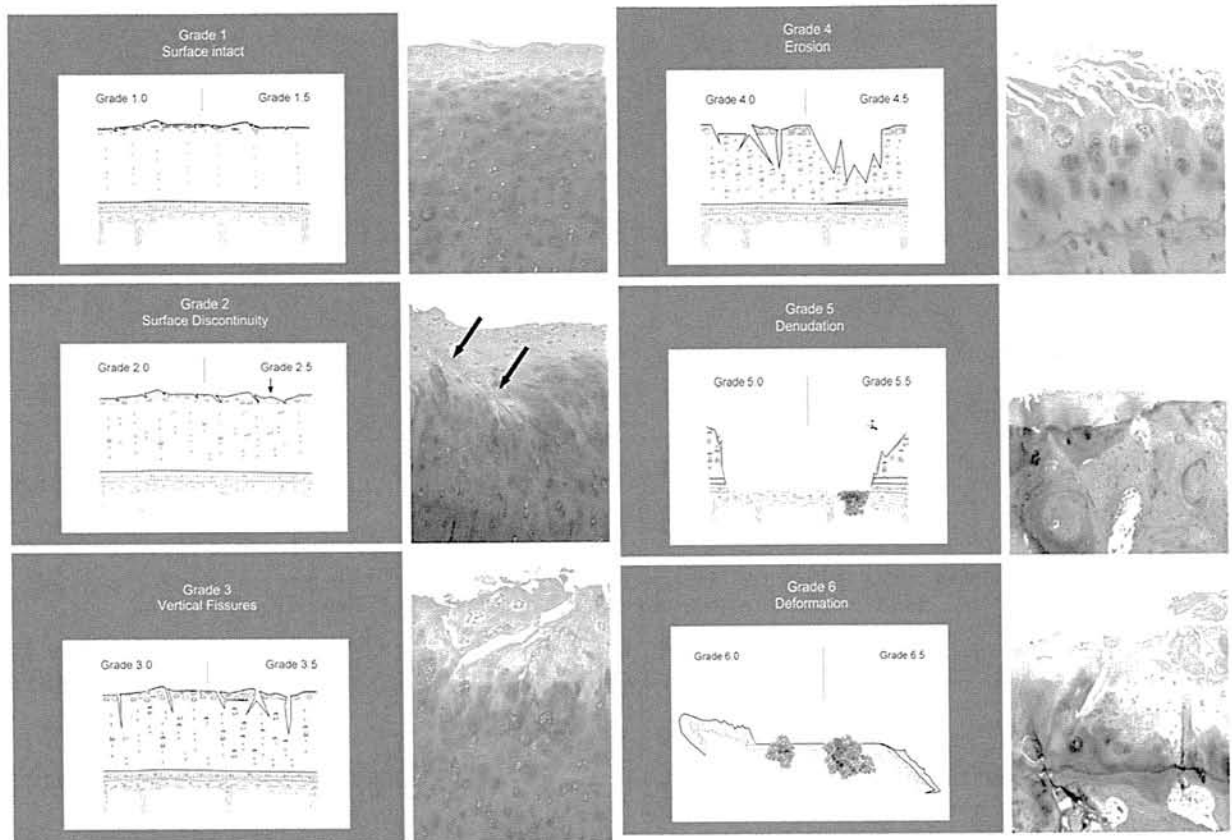


**Fig. 2-4** Terminal case of OA

The typical case appearance (a), Roentgenogram of after TKR (b) [4]

Increasing grade indicates progression of OA (**Fig. 2-5**). The progress of the disease is demonstrated and graded pathologically as follows; grade 1: uneven surface and superficial fibrillation, grade 2: superficial discontinuity and focal fibrillation, grade 3: vertical fissures extending into mid zone, grade 4-6: destruction of the cartilage.





**Fig. 2-5** OA cartilage pathology (Safranin O stain) [5].

Safranin O stain, original magnification  $\times 5$ .

## 2.3 Evaluation of OA

OA changes of the knee joints are diagnosed and graded either with plain radiographs using K-L scoring system and/or arthroscopy and/or MRI using Outerbridge or modified Outerbridge classification. As a new approach, quantitative assessment of the cartilage using MRI is under investigation.

### 2.3.1 Initial consultation

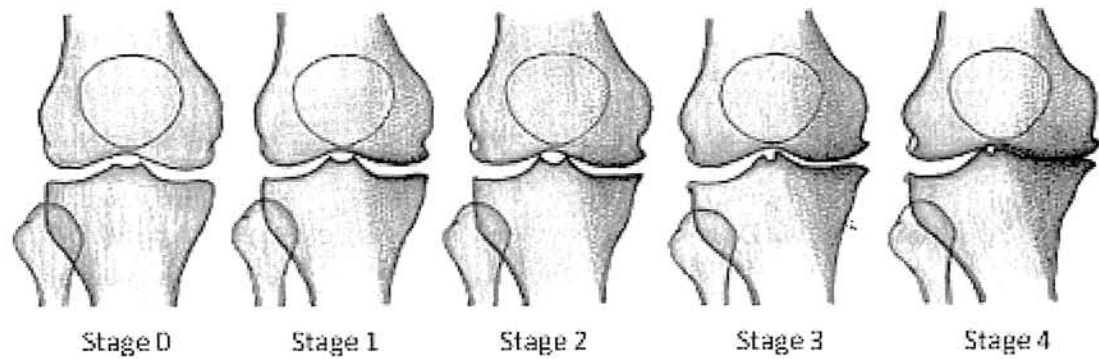
The evaluation of osteoarthritis of the knee is investigated by assessment Japanese orthopedics society OA knee treatment result criteria (JOA score), Western Ontario and McMaster Universities Osteoarthritis Index (WOMAC) or Japanese Knee Osteoarthritis Measure (JKOM). Biochemical tests such as urine sampling or blood drawing are carried out following an interview.

### 2.3.2 Kellgren-Lawrence Score

Diagnosis of knee osteoarthritis (OA) is typically performed though identification of bone changes and joint space narrowing on radiographs is using the Kellgren-Lawrence (KL) scoring system [6]. This indirect measure of cartilage disease is likely preferred due to its relatively low cost and minimal requirements in analysis time. However, the earliest changes in cartilage degeneration are alterations in the biochemistry of the extracellular matrix of the cartilage and are unlikely to be observed on radiographs [7]. Stage 0 indicates no radiographic findings of osteoarthritis, stage 1 minute osteophytes of doubtful clinical significance, stage 2 definite osteophytes with unimpaired joint space, stage 3 definite osteophytes with moderate joint space narrowing and stage 4 definite osteophytes with severe joint space narrowing and



subchondral sclerosis (**Fig. 2-6**).

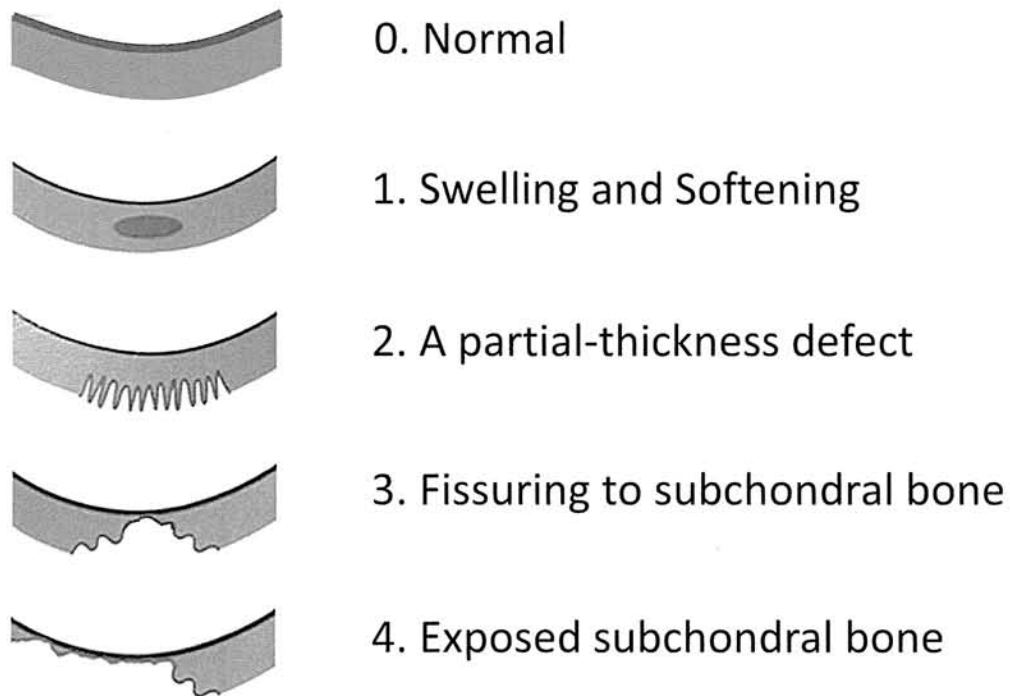


**Figure 2-6** Schematic illustration of Kellgren-Lawrence Score

([http://www.juntendo.ac.jp/hospital/clinic/seikei/kanja02\\_b.html](http://www.juntendo.ac.jp/hospital/clinic/seikei/kanja02_b.html))

### 2.3.3 Outerbridge classification

The Outerbridge classification (**Fig. 2-7**) is a grading system for joint cartilage breakdown. The Outerbridge classification is an invasive diagnostic method using arthroscopy, and elastic evaluation by an indenter is also performed simultaneously.



**Fig. 2-7** Schematic illustration of Outerbridge classification [3]

#### 2.3.4 Modified Outerbridge classification using MRI

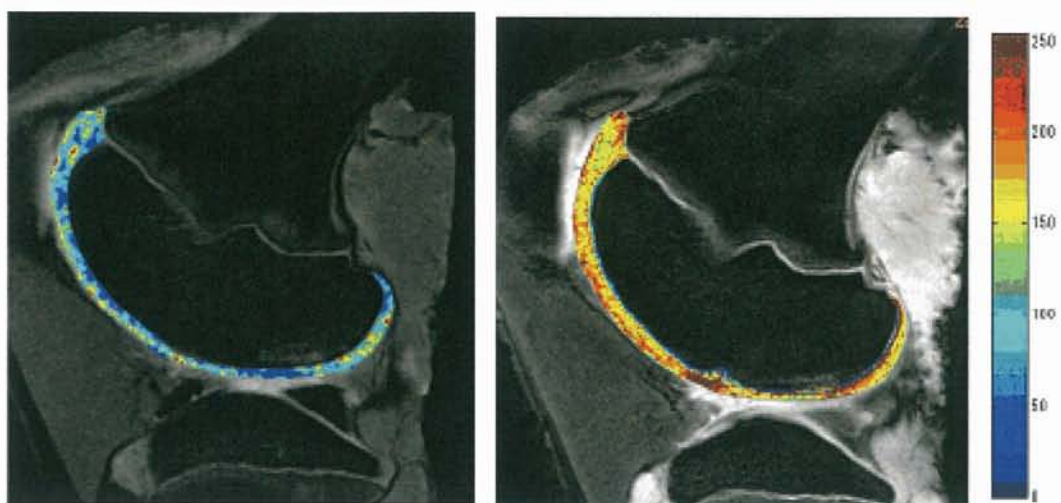
The Modified Outerbridge classification is a grading system in arthroscopy for joint cartilage injury using MRI based on the Outerbridge classification.

In modified Outerbridge classification, Grade 0 indicates intact cartilage, grade 1: chondral softening or blistering with an intact surface, grade 2: shallow superficial ulceration, fibrillation, or fissuring involving less than 50 per cent of the depth of the articular surface, grade 3: deep ulceration, fibrillation, fissuring or a chondral flap

involving 50 per cent or more of the depth of the articular cartilage without exposure of subchondral bone and grade: full-thickness chondral wear with exposure of subchondral bone [8].

#### 2.3.5 Quantitative cartilage imaging using MRI

Various proton relaxation times can be quantitatively measured in the articular cartilage. Recently, with three different MR techniques, measurements of longitudinal, transverse relaxation times and spin-lattice relaxation time in the rotating frame (**Fig. 2-8**), have been reported. T1 is always measured after intra venous administration of gadolinium-diethylene triamine pentaacetic acid (Gd-DTPA). The delayed gadolinium enhanced magnetic resonance imaging (MRI) of cartilage (dGEMRIC) is obtained and demonstrates preferential accumulation of the negatively charged contrast agent in cartilage with decreased PG content that causes diminution of proton T1 compared with normal tissue. Transverse relaxation time (T2) is proportional to the distribution of cartilage water and is inversely proportional to the concentration of PG. Spin-lattice relaxation time in the rotating frame (T1 $\rho$ ) correlates to PG content in articular cartilage and it is more sensitive to the change of PG than T2 [9].



**Fig. 2-8** the quantitative image of the cartilage by relaxation time  
T2-mapping (a) and T1ρ-mapping (b) in a porcine model.



## Chapter 3 Microscopic water molecule motion in the cartilage obtained from diffusion weighted images

### 3.1 Free diffusion

Molecular diffusion refers to the random translational motion of molecules called Brownian motion, which results from the thermal energy carried by these molecules [1]. The movement of molecules causes normal probability distribution, and the quantity of movement of molecules is proportional to concentration gradient macroscopically. This proportional constant is diffusivity  $D$  which is based on a particular solution of the diffusion equations (1).

$$\frac{\partial C(x,t)}{\partial t} = D \frac{\partial^2 C(x,t)}{\partial x^2} \quad (1)$$

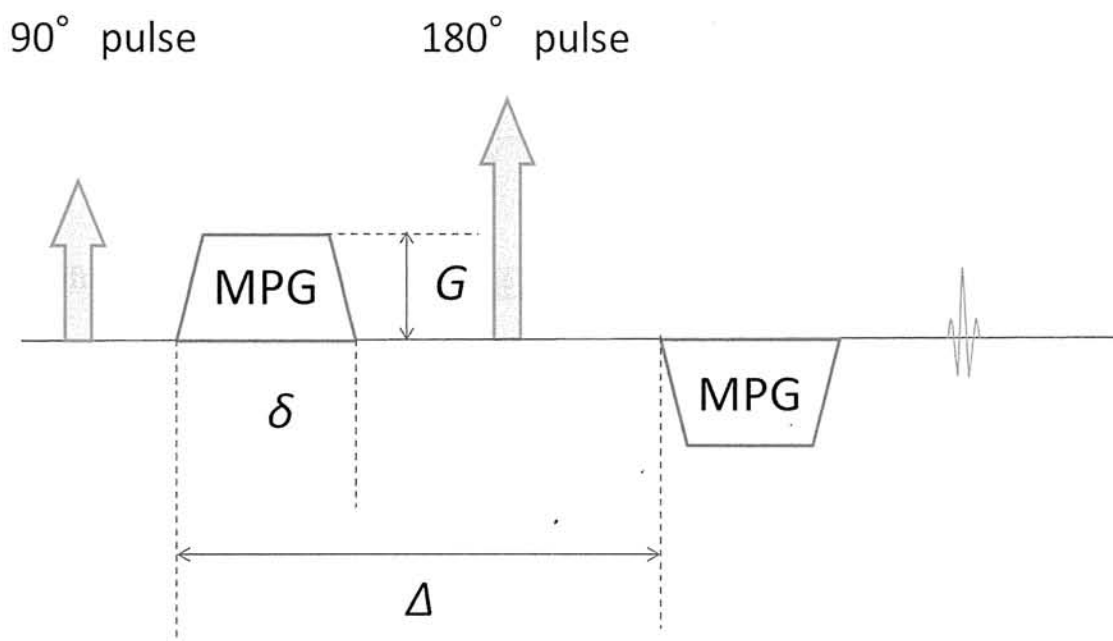
One of the special solutions of the diffusion equation shows normal distribution in point spread function (2).

$$\frac{1}{\sqrt{4\pi Dt}} \exp\left[-\frac{x^2}{4Dt}\right] \quad (2)$$

Another special solution of the equation shows a sine wave in frequency response.

$$\exp[-Dk^2t] \sin kx \quad (3)$$

The distribution of magnetization made in a gradient magnetic field shows the solution of the diffusion equation. The signal intensity decays exponentially but the shape of the distribution with time is unchangeable, and the degree of the decay signal depends on diffusivity  $D$  and spatial frequency  $k$ . The diffusion weighted image uses bipolar gradient in Echo Planner Imaging (EPI) sequence (**Fig. 3-1**). Bipolar gradient i.e., motion probing gradient (MPG) causes dephasing of spins by the first gradient.



$G$ : magnitude of the gradient,  $\delta$ : time to apply of MPG (diffusion time),  $\Delta$ : interval between MPG

**Fig. 3-1** Schematic representation of diffusion weighted image sequence

Stationary tissue is rephased at the end of the second opposite MPG; therefore, stationary tissue reveals high signal intensity. In tissue with molecular movement of

water protons, a signal loss occurs since the protons have moved out by the time of the rephasing opposite gradient. The greater the mean free path length of the water molecules, the greater is the signal loss achieved with a diffusion-weighted sequence.

The strength of MPG is given with a  $b$  value in the following equation;

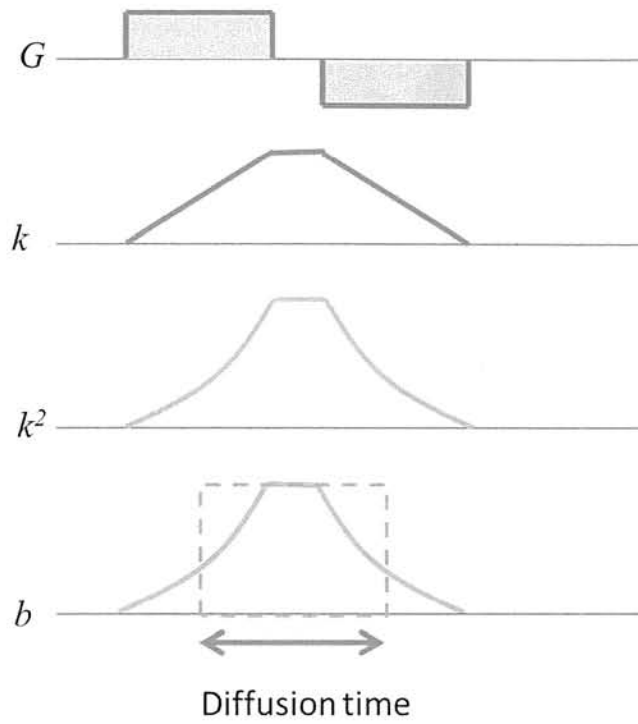
$$k = \int_0^t \gamma G dt' \quad (4)$$

$$b = \int_0^T k^2 dt$$

$$b = \gamma^2 G_x^2 \delta^2 \left( \Delta - \frac{\delta}{3} \right) \quad (\text{s/mm}^2) \quad (5)$$

**Figure 3-2** shows relations of  $k$  and  $b$  value in applying bipolar gradient. The diffusion phenomenon applies to random movement (incoherent motion) of innumerable protons. The diffusion weighted image is influenced by coherent motion and cannot distinguish coherent motion from incoherent motion in voxel. The strength of MPG is indicated by  $b$  value. Since strong MPG reduces the signal of the fast moving molecules, application of high  $b$  value is suitable to assess slowly moving molecules. Amplitude of the  $b$  value has a trade-off relation with the signal intensity, as well as, defines the image contrast. From the special solution of the diffusion equation using sine wave, the change of the signal intensity is given in a following expression;

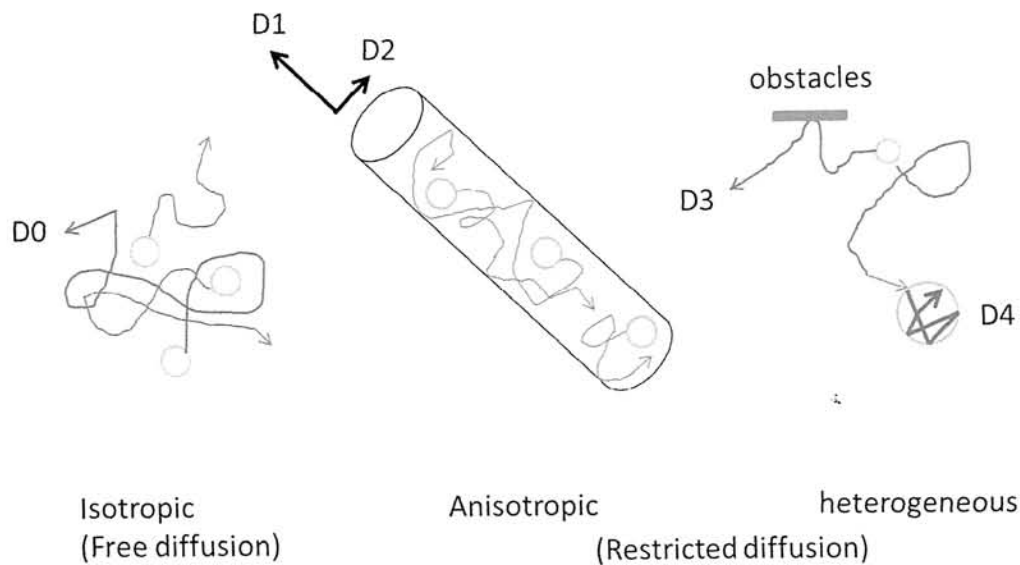
$$\exp\left[-D\int_0^t k^2 dt'\right] = \exp[-bD] \quad (6)$$



**Fig. 3-2** Schematic representation of  $G$ ,  $k$ ,  $b$

### 3.2 Restricted diffusion

For example, the movement of molecules in vivo is limited by a cell membrane (anisotropic diffusion) and does not move freely (**Fig. 3-3**).



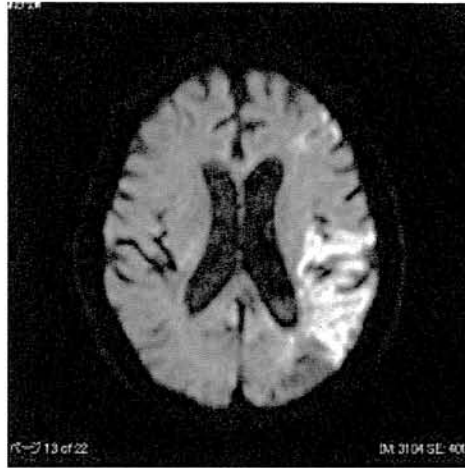
**Fig. 3-3** Schematic representation of the interaction of diffusing molecules with various types of obstacles or constraints to free diffusing motion.

Isotropic diffusion is restricted as anisotropic or heterogeneous in human body

$$(D_0 > D_1 > D_2, D_0 > D_3 > D_4).$$

Apparent diffusion coefficient (ADC) is distinguished from diffusivity  $D$ , since it represents the anisotropic diffusion of water molecules in vivo. ADC is calculated from two or more images obtained by different  $b$  values. The contrast in the ADC map depends on the spatial distribution of ADC and does not contain T1 and T2\* values.

MRI can demonstrate the state of diffusion phenomenon in human body which is applied in a variety of clinical settings, especially in acute cerebral stroke at the posterior part of the left middle cerebral arterial territory (**Fig. 3-4**).



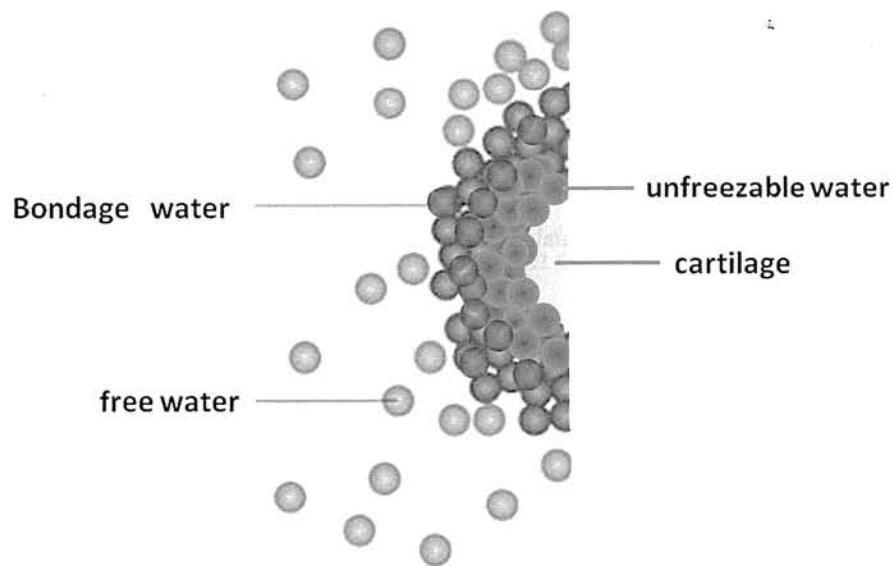
**Fig. 3-4** Diffusion weighted image of acute ischemic stroke

(Reference cited: Kumamoto general Hospital, [http://www.cityhosp-kumamoto.jp/xsen/pg-MRI\\_00.html](http://www.cityhosp-kumamoto.jp/xsen/pg-MRI_00.html))

### 3.3 Diffusion in articular cartilage

Articular cartilage is a bi-phasic material: the permeable solid section which is represented by a solid matrix that consists of collagen fibers and proteoglycan molecules, and the fluid section which is composed of extracellular water with dissolved ions and nutrients. Diffusion weighted imaging may offer information that is related to the integrity of the collagen network by investigating the nature of fluid dynamics in cartilage through its ability to distinguish between moving and stationary fluids [2]. Most of the fluid (**Fig. 3-5**) can move through the collagen network during loading. When the bound water restricted by a collagen network and proteoglycan is

subjected to loading, especially at weight bearing joints such as knee joints. When load is removed, the free water invades again, and the cartilage has the elasticity and the property of viscosity by this action.

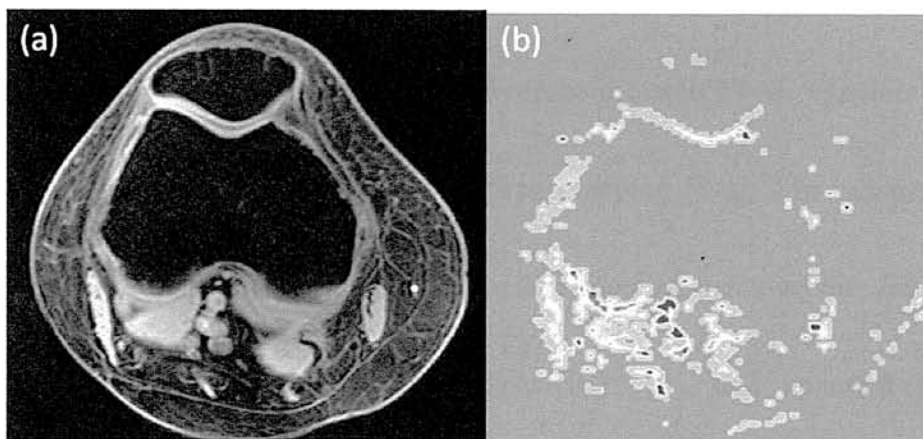


**Fig. 3-5** Schema of fluid in articular cartilage model

As the way, the fluid dynamics in conjunction with the pore morphology and fluid transportation plays an important role in the overall mechanical function of the joint and ADC may become a new approach to diagnosis [3]. Macromolecules in the cartilage restrict the displacement of water compared with in bulk water; therefore the ADC is generally lower in cartilage than in bulk water. Burstein et al. reported increases in ADC following enzymatic degradation of cartilage with trypsin, while

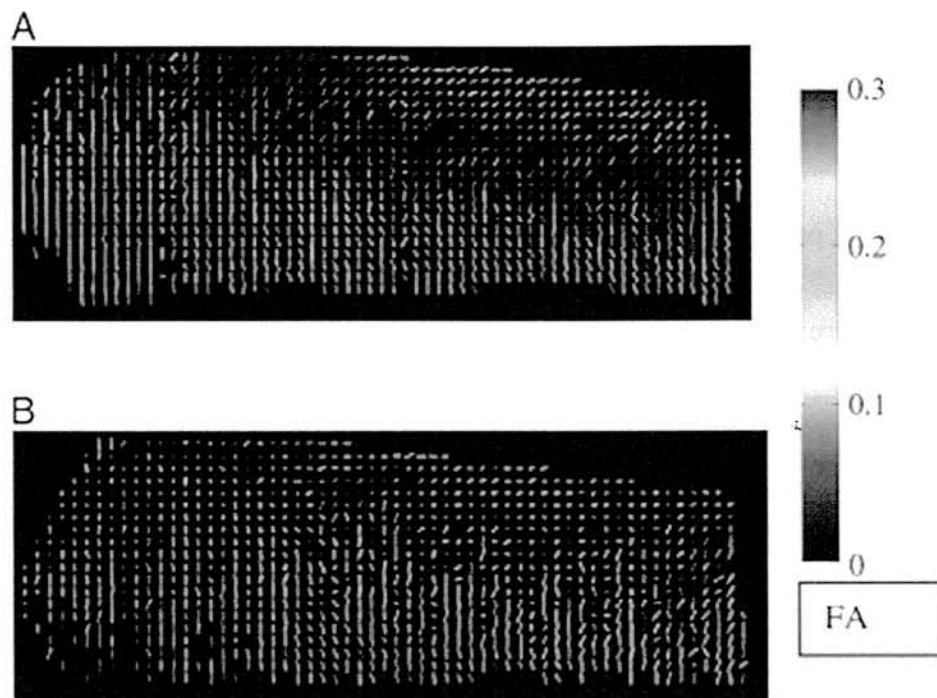


mechanical compression of the tissue resulted in a reduction in ADC [4]. Zhu et al. reported both the DWI images and the ADC can provide insights into physiologic characteristics of patellar cartilage in vivo (**Fig. 3-6**). DWI reflects the microscopic of the tissue structure by water molecules that are undergoing random diffusion-driven movements. The collagen fiber of cartilage is anisotropic architecture [5], and the self-diffusion of the water protons is characterized by a  $3 \times 3$  tensor [6]. The Diffusion Tensor Imaging (DTI) can measure diffusion anisotropy of in vivo cartilage and the direction of the eigenvectors corresponding to maximum diffusion reflects the alignment of collagen fibers [7] (**Fig. 3-7**).



**Fig. 3-6** Morphological image and ADC mapping of the knee.

Morphological T2star transverse image (a) and ADC-mapping of the knee (b). The ADC values were represented by different colors on the color maps of ADC; green areas were cartilage (b).



**Fig. 3-7** DTI of human articular cartilage.

Baseline-preferred diffusion direction map (A). Preferred diffusion direction map for the same sample after treatment with trypsin and collagenase (B). Reference cited: Deng X et al. / MRI 2007.

## **Chapter 4** Evaluating relation between apparent diffusion coefficient and viscoelasticity of the cartilage

### 4.1 Introduction

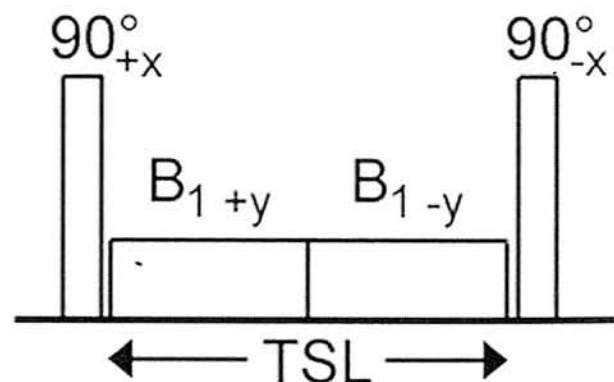
In the early stages of OA, conservative treatment is often recommended to prevent the progression of degenerative changes in articular cartilage. These changes include the disruption and/or alteration of the extracellular matrix, in such forms as decreased concentration of proteoglycans, increased water content, or deterioration of collagenous architecture, all of which have been demonstrated biologically and histologically [1-2]. The application of quantitative MR imaging techniques to degenerative cartilage has been a focus of recent research [3-4]. Quantitative MR imaging techniques, such as T2 relaxation time mapping [5-6], T1ρ relaxation time mapping [7-9], delayed gadolinium-diethylene-triamine-penta-acetic (Gd-DTPA)-enhanced MR imaging of cartilage (dGEMRIC) [10], and apparent diffusion coefficient (ADC) mapping [11], have been reported as useful indicators of degenerative changes in cartilage extracellular matrix, which consists of proteoglycans, collagen, non-collagenous proteins, and water. T2 measurements in cartilage have been

shown to correlate with collagenous architecture and water content [5], while T1 $\rho$  measurements in cartilage have been shown to correlate with proteoglycans and water content [12]. The dGEMRIC technique has been shown to correlate mainly with proteoglycans. ADC measurements, on the other hand, have been shown to correlate mainly with water content and collagen matrix structure in cartilage. [13-14]. It has been shown that water and the collagen matrix produce the flow-dependent viscoelasticity of cartilage [15]. Thus, ADC can serve as an ideal indicator of the viscoelasticity of cartilage. Several studies have addressed the relationship between ADC and viscoelasticity. Juras et al. reported that ADC correlates with relaxation time in superficial zones using specimens in different stages of degeneration from patients who had undergone total knee replacement surgery [16]. Topographic variation in the cartilage matrix has also been shown to exist [17-19]: weight-bearing regions receive direct compression and tensile loading during walking, while non-weight-bearing regions receive less loading. Yet topographic variation in terms of ADC and viscoelasticity has not been previously studied. The aim of this study was to investigate correlation between ADC, T1 $\rho$  and the viscoelasticity using porcine knee cartilage.

## 4.2 Theory supported T1ρ

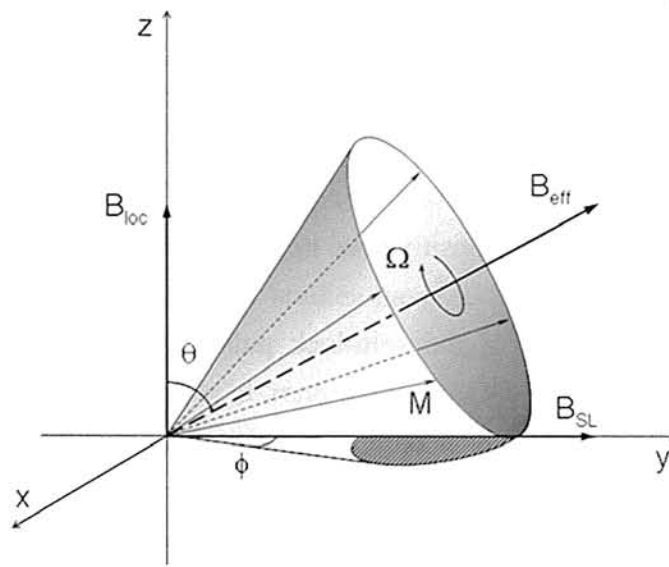
### 4.2.1 Spin-Lock pulse

The initial nonselective  $90^\circ$  pulse along the  $+x$  axis nutates the magnetization into the transverse plane along the  $+y$  axis. The magnetization vector is then spin-locked with amplitude  $B_1$  for a duration of TSL with an on-resonance spin-lock pulse applied in line with the magnetization vector along the  $y$  axis. The spin-lock pulse is split into two phase-alternating halves along the positive and negative  $y$  axes to reduce the effects of  $B_1$  inhomogeneity. At the end of the spin-lock pulse, the magnetization vector is nutated back into the longitudinal axis using a nonselective  $90^\circ$  pulse along the  $-x$  axis. This pulse cluster is preencoded before a read-out sequence to create a single-slice spin-lock pulse sequence (**Fig. 4-1**) [20].



**Fig. 4-1** Schematic of a T1ρ-weighted spin-lock RF pulse cluster

The equilibrium longitudinal magnetization  $M_0$  is tilted to the transverse plane by a  $90^\circ$  RF pulse. This is followed immediately by a locking RF pulse BSL, which is applied during the locking time TSL. The phase of BSL is adjusted so that it is parallel aligned with the tilted magnetization vector  $M$  (**Fig. 4-2**) [21].



**Fig. 4-2** Magnetization vector  $M$  during the SL pulse with amplitude  $B_{SL}$  in an inhomogeneous field  $B_{loc}$ .

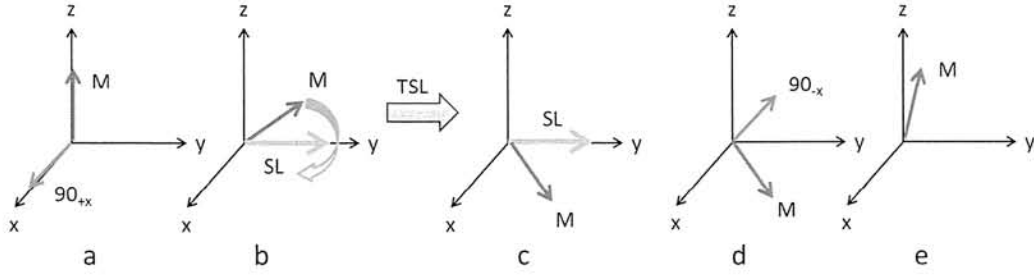
#### 4.2.2 Magnetization in the rotating frame

T1ρ pre-pulse sequence consists of a  $90^\circ_y$  pulse to bring the magnetization along (for example) the  $x'$ -axis, followed by a long “lock” pulse, exciting a  $B_1$  field along the  $x'$ -axis. This lock pulse prevents T2 dephasing of spins. The spins are after some time

brought back in the longitudinal direction with a  $90^\circ$  “flip-up” pulse. During the locking pulse there is interaction of the free water proton spins with the spins of the macromolecules, causing  $T1\rho$  decay depending on the relative amount of macromolecules and their properties, somewhat similar to the processes governing magnetization transfer contrast (MTC). This prepulse was originally applied at very low fieldstrength, where the inhomogeneties of the main magnetic field are unimportant. At high fieldstrength with large absolute values of field inhomogeneities, a composite  $T1\rho$  prepulse yields better locking [22].

The magnetization (M) begins along the z-axis in the equilibrium position (a) and is nutated into the y-axis by the initial hard  $90^\circ$  along the x-axis. The magnetization then nutates in the rotating frame about the SL pulse applied along the y-axis (b). At the end of the spin-lock pulse duration (TSL), the magnetization is left in the transverse plane (c). The magnetization is then restored to the longitudinal axis by the second hard  $90^\circ$  applied along the negative x-axis (d). The resultant  $T1\rho$ -prepared magnetization is ready to be read using gradient echo (GRE) or spin echo (SE) readout. Residual transverse magnetization is destroyed using a crusher gradient immediately following the second hard  $90^\circ$  pulse (**Fig. 4-3**) [20].





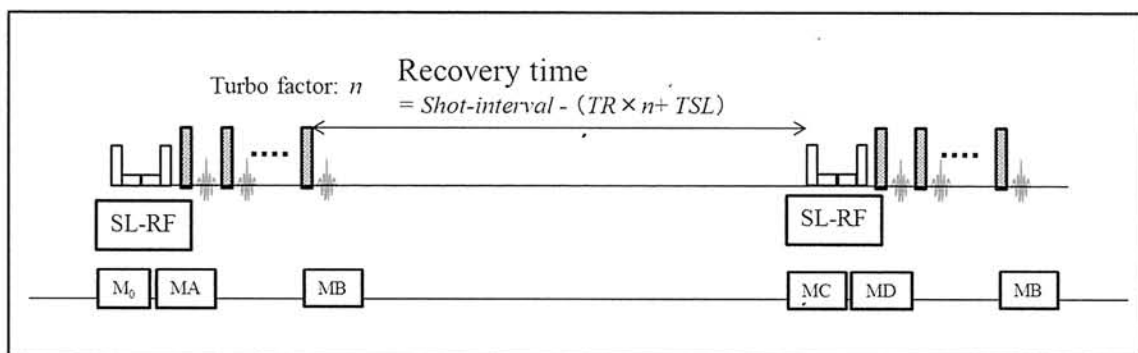
**Fig. 4-3** Vector diagram of the nutation of the magnetization in the rotating frame of reference.

T1 $\rho$  mapping is a quantitative MRI technique that has been used to evaluate degenerative changes in the extracellular matrix of cartilage [23]. T1 $\rho$  can be measured through a combination of pulse sequences designed to obtain spin-lock pre-pulse and contrast. T1 $\rho$  sequences are typically combined with readout sequence such as three-dimensional (3D) GRE sequences [24-26] to decrease both the scan time and the specific absorption rate (SAR) [20, 24].

#### 4.2.3 T1 $\rho$ -prepared segmented multi-shot 3D-TFE sequence

The pulse sequence diagram is shown in **Fig. 4-4**. Initial longitudinal magnetization ( $M_0, t = 0$ ), spin-lock RF pulse (SL-RF), post SL-RF longitudinal magnetization ( $M_A, t = t_a$ ), longitudinal magnetization after  $n$  RF pulses ( $M_B, t = t_b$ ), recovered longitudinal magnetization ( $M_C$ ), and post-SL-RF longitudinal magnetization ( $M_D$ ).

Recovery time ( $t$ ) = shot interval - ( $TR \times n + TSL$ )  $> T1 \times 5$ . Longitudinal magnetization changes from  $M_0$  to  $MA$ ,  $MB$ ,  $MC$ , and  $MD$ . T1p weighted signals were recorded during the transient state to avoid measurements during a steady state. The signal intensity was measured when the  $k$ -space was filled from low to high (in centric order) immediately after the spin-lock signal (MD) fills  $k = 0$ . The time required to reach steady state depends on the T1 value of the tissue; in tissues with a short T1, such as adipose tissue, steady state can be achieved immediately. In contrast, in tissues with a long T1, such as water, the transient state continues until the end of the data collection period.



**Fig. 4-4** Schematic diagram of the common T1p prepared GRE sequence

Changes in the longitudinal magnetization of each period are given by the following formulas:

$$MA = M_0 \times e^{(-TSL / T1\rho)}$$

$$MB = MA \times e^{-\left(\ln(\cos \alpha) + \frac{TR \times n}{T1}\right)} + \frac{TR \times n \times M_0}{T1 \times \ln(\cos \alpha) + TR \times n} \left(1 - e^{-\left(\ln(\cos \alpha) + \frac{TR \times n}{T1}\right)}\right)$$

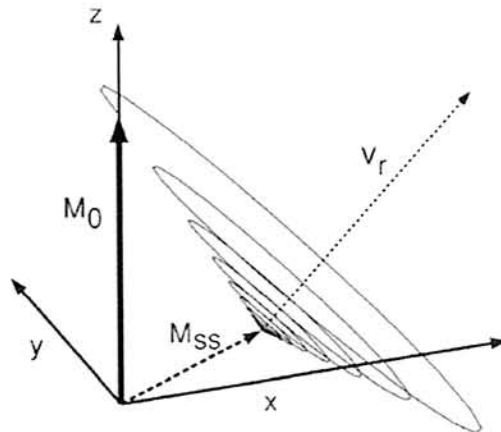
$$MC = M_0 \left(1 - \left(1 - MB / M_0\right) \times e^{-\text{Recovery time} / T1}\right)$$

$$MD = MC \times e^{(-TSL / T1\rho)}$$

where  $\alpha$  is the flip angle and  $n$  is number of RF pulses (TFE factor).

#### 4.2.4 Behavior of the magnetization of the transient period

The transient response (**Fig. 4-5**) is the magnetization during the initial period of a sequence during which steady-state magnetization  $\mathbf{M}_{ss}$  evolves from a particular initial condition. The length and character of the transient response depends on  $T1\rho$ ,  $T2\rho$ , and the initial condition,  $\mathbf{M}_0$  [27].

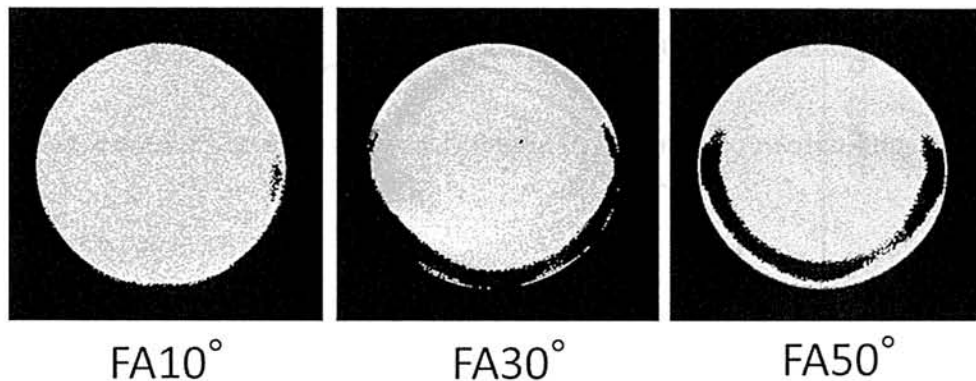


**Fig. 4-5** Transient response of magnetization from  $\mathbf{M}_0$  to  $\mathbf{M}_{ss}$

The real-valued eigenvector,  $\mathbf{V}_r$ , is shown. The component of the transient response which is directed along  $\mathbf{V}_r$  decays exponentially. The component that is orthogonal to  $\mathbf{V}_r$  decays along a circular spiral path in the plane almost orthogonal to  $\mathbf{V}_r$ .

#### 4.2.5 Artifact

If the magnetization vector is poorly aligned with the spin-locking pulse, there is ample opportunity for it to undergo pronounced off-axis nutation. This occurs in the case of an inhomogeneous  $B_1$ , where nutation angles are spatially varying and may result in dramatically non-uniform image artifacts that markedly degrade any attempts at quantitative imaging (**Fig. 4-6**).



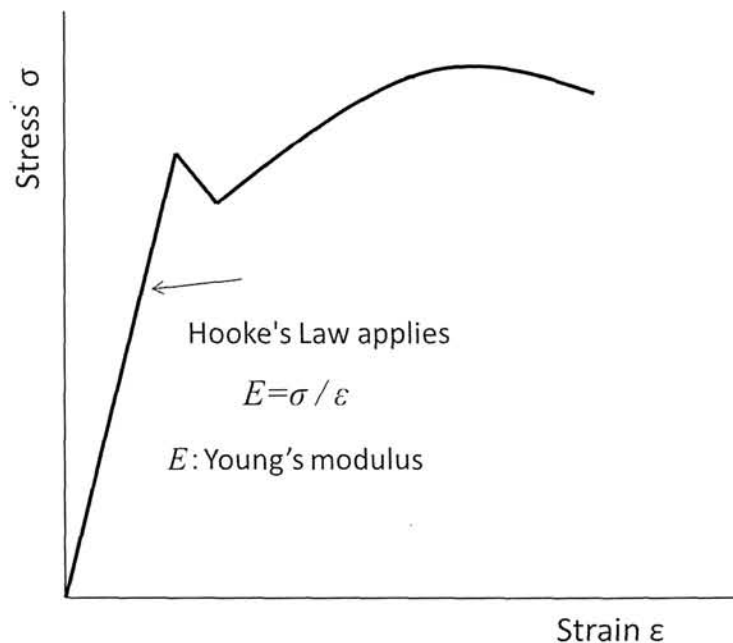
**Fig. 4-6** Artifact of the phantom image depending on the FA

## 4.3 Basic points of mechanical property

### 4.3.1 Viscoelasticity

Viscosity is a measure of the resistance of a fluid which is being deformed by either shear stress or tensile stress. Water is a lower viscosity, while honey is a higher viscosity. The less viscous the fluid is, the greater its ease of movement (fluidity).

Young's modulus, also known as the tensile modulus or elastic modulus, is a measure of the stiffness of an elastic material and is a quantity used to characterize materials. It is defined as the ratio of the uniaxial stress over the uniaxial strain in the range of stress.



**Fig. 4-7** Stress-Strain Curve

Viscoelasticity is the property of materials that exhibit both viscous and elastic characteristics when undergoing deformation. Viscous materials, like honey, resist shear flow and strain linearly with time when a stress is applied. Elastic materials strain instantaneously when stretched and just as quickly return to their original state once the stress is removed. Viscoelastic materials have elements of both of these properties and, as such, exhibit time-dependent strain.

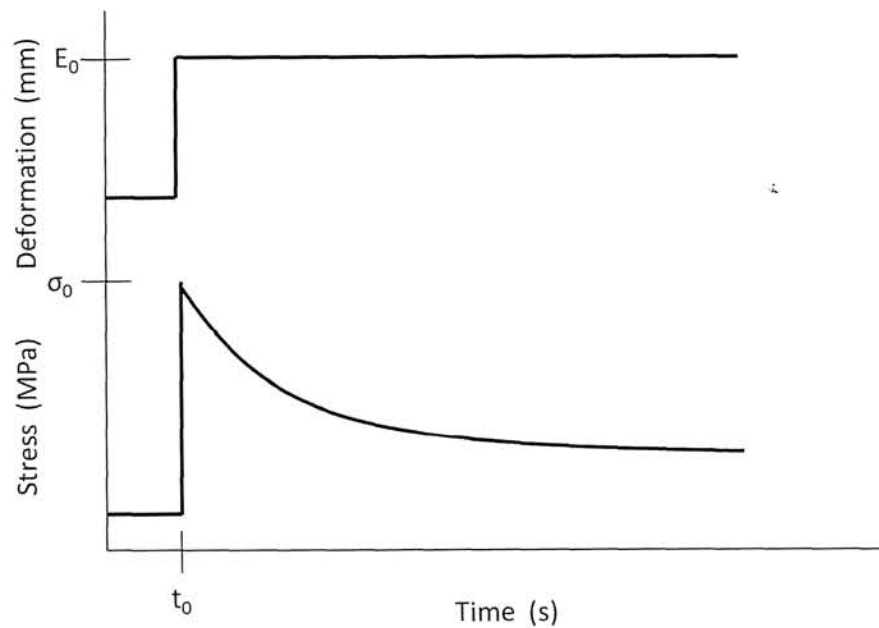
#### 4.3.2 Effect of temperature on viscoelastic behavior

Thermal motion is one factor contributing to the deformation of polymers, viscoelastic properties change with increasing or decreasing temperature. An increase in temperature correlates to a logarithmic decrease in the time required to impart equal strain under a constant stress.

#### 4.3.3 Stress relaxation

Stress relaxation describes how polymers relieve stress under constant strain. Because they are viscoelastic, polymers behave in a nonlinear.

This nonlinearity is described by both stress relaxation and a phenomenon known as creep, which describes how polymers strain under constant stress.



**Fig. 4-8** Stress-Relaxation Curve

**Figure 4-8** shows the response of a Standard Linear Solid material to a constant stress,

$\sigma_0$ , over time from  $t_0$  to a later time  $t_f$ . For times greater than  $t_f$  the load is removed.

The curvatures of the model represent the effects of both creep and stress relaxation.



## 4.4 Material and Methods

### 4.4.1 Subjects

Fresh porcine knee joints (n =20, age 6 months) were obtained from a local abattoir (ZEN-NOH Central Research Institute for Feed and Livestock, Ibaraki, Japan). Because we used branded edible pigs, which for quality-control purposes are slaughtered precisely six months after birth, all pigs had almost finished growing but remained skeletally immature.

### 4.4.2 MR Imaging

MR imaging was performed within 30 hours after euthanasia. Specimens were kept at room temperature (20°C) for three hours before MR imaging. MR imaging was performed on a 3.0-T whole-body clinical scanner (Intera Achieva; Philips Medical Systems, Best, Netherlands) with an 8-ch SENSE (sensitivity encoding) knee coil using a parallel imaging technique. Sagittal MR images were acquired along a plane perpendicular to the line which passes through the medial femoral condyle and the lateral femoral condyle. In this plane, we did not evaluate the tibial and patellar cartilage to avoid any partial volume effect due to surrounding structures. Morphological isotropic

images were acquired using a three-dimensional fast field echo (3D-FFE) sequence, ADC of cartilage was measured using a single-shot spin echo-echo planar image sequence and three-dimensional T1ρ prepared turbo field echo (3D-TFE) sequence showed in **Table 4-1**, where repetition time: TR, echo time: TE, field of view: FOV, excitations: NEX, spin lock time: TSL, flip angle: FA.

**Table 4-1** Scan parameters

	3D-FFE	ADC	T1ρ
TR/TE1/TE2	19/7.0/13.3 ms	4000/47	12/9.2
FOV	150	120 x 120	120
Matrix (interpolated matrix)	256 x 256 (512 x 512)	128 x 128 (256 x 256)	256 x 256
Slicethickness/ gap/Number	0.3mm/ 0/250 Isotropic voxel	3 mm/0.3 mm/19	3 mm/0 mm/19
NEX	1	1	1
<i>b</i>		0,700,1000,1500 s/mm <sup>2</sup>	
TSL			1,10,20,40,80 ms
FA/ spin lock amplitude	35 degree	90 degree	10 degree/ 500 Hz
Total Acq.time	5'09"	1'48"	2'21"(each TSL)

An ADC map was generated from diffusion weighted images using the built-in software that accompanies the clinical scanner (Philips). An ADC map was generated

on a pixel-by-pixel basis by fitting the  $b$  value data from the measured signal intensity ( $S_b$ ) attenuation according to a mono-exponential decay equation, as follows:

$$S_{(b)} = S_{(b=0)} \exp(-bD)$$

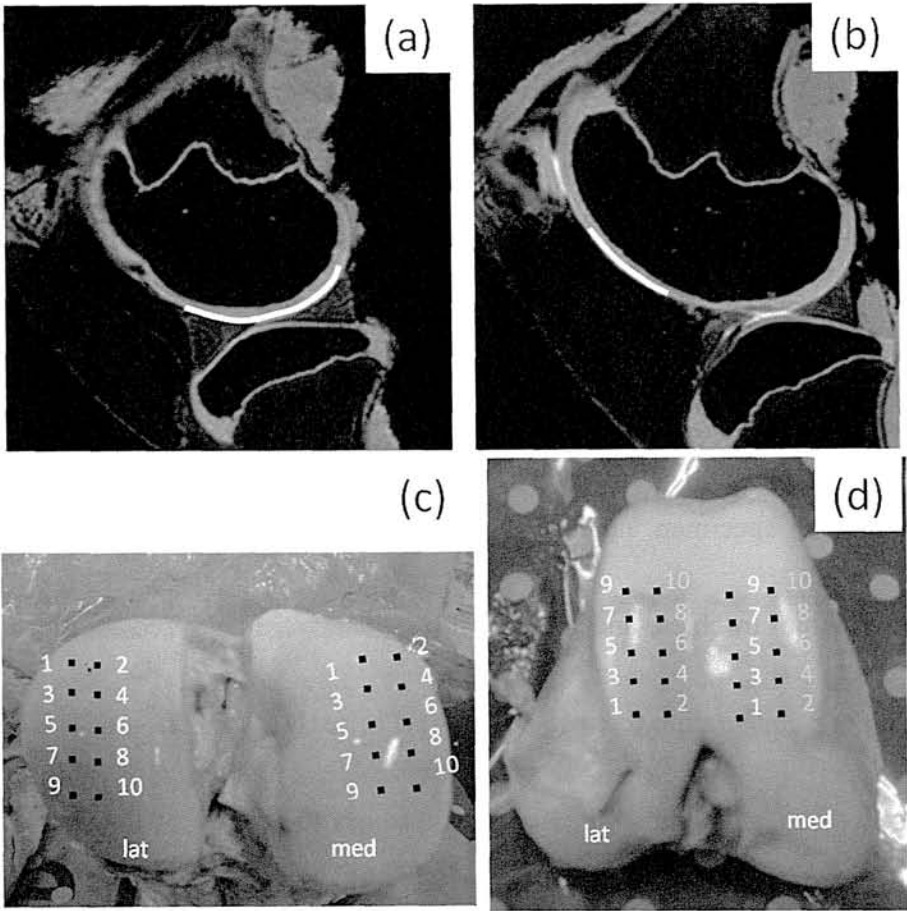
A T1 $\rho$  map was generated on a pixel-by-pixel basis by fitting the  $TSL$  value data from the measured signal intensity ( $S_{TSL}$ ) attenuation according to a mono-exponential decay equation, as follows:

$$S_{(TSL)} = S_{(TSL=0)} \exp(-TSL / T1\rho)$$

#### 4.4.3 ROI setting

Four sites in each specimen, namely, the medial femoral condyle, the lateral femoral condyle, the medial trochlea, and the lateral trochlea, were analyzed by means of both MR imaging and indentation testing (**Fig. 4-9**). For each specimen, a region of interest (ROI) was drawn on the slice which passed through the center of the medial femoral condyle, the lateral femoral condyle, the medial trochlea, and the lateral trochlea. This ROI was drawn to include the weight-bearing area of the medial and lateral condyles and the non-weight-bearing area of the medial and lateral trochleae. Furthermore, the cartilage was divided along a line parallel to the cartilage/bone interface into two layers (superficial and deep) of equal thickness. An ROI was drawn over the entire superficial

layer as it has been shown that degenerative changes begin in the superficial layer, and also because mechanical testing mainly reflects the properties of the superficial layer of cartilage. All ROIs were drawn manually by a single investigator.

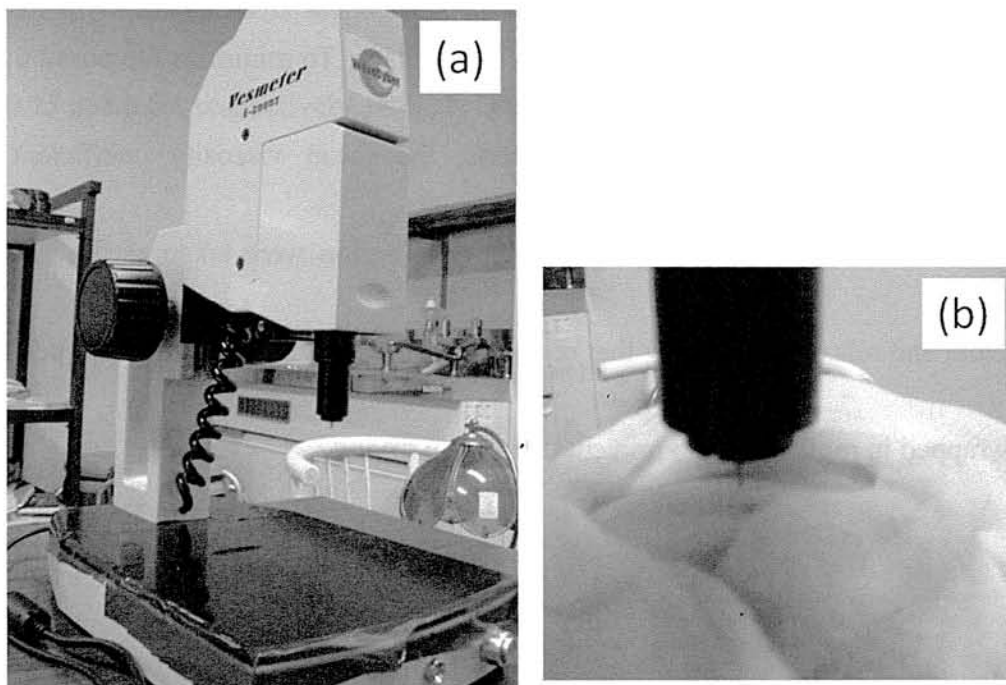


**Fig. 4-9** Image of the ROI

MR image of weight-bearing region (a) and non-weight-bearing region (b), Indenter testing points of weight-bearing region (c) and non-weight-bearing region (d)

#### 4.4.4 Mechanical testing

Indentation testing (**Fig. 4-10**) was performed on an electromechanical precision controlled system (Vesmeter E-200DT; WaveCyber Co., Ltd., Saitama, Japan). The shape of the indenter tip is a cone with an angle of 30 degrees, a tip diameter of 0.1 mm, and a pressurization of 35 grams each 0.2 second. Measuring one region takes less than 2 minutes.



**Fig. 4-10** Image of the indenter test device

Indentation testing device (a) and the appearance under measurement of porcine knee cartilage in situ (b). A shape of the tip of the indenter is cone of 30 degrees, tip diameter of 0.1 mm, and pressurization of 35 gram.

This device can provide the viscosity, elasticity, relaxation time, elastic rate, stiffness, and strain depth as given by Voigt's equation:

$$S = G\gamma + \eta \cdot \frac{d\gamma}{dt}$$

where  $\gamma$  denotes displacement,  $G$  is elastic modulus,  $\eta$  denotes viscosity and  $S$  is stress.

Indentation testing was performed on the same regions that were selected for MRI analysis. Two lines consisting of five points per line at intervals of 3 - 4 mm were tested for a total of 10 points in each region. Viscosity coefficient and relaxation time were measured as indicators of the viscoelasticity of cartilage. To minimize the possibility of measurement errors during indentation tests, the mean viscosity coefficient and relaxation time obtained for all ten points in each region were taken as the viscosity coefficient and relaxation time for that region. During mechanical testing, the specimens were wrapped in moist gauze to prevent them from drying.

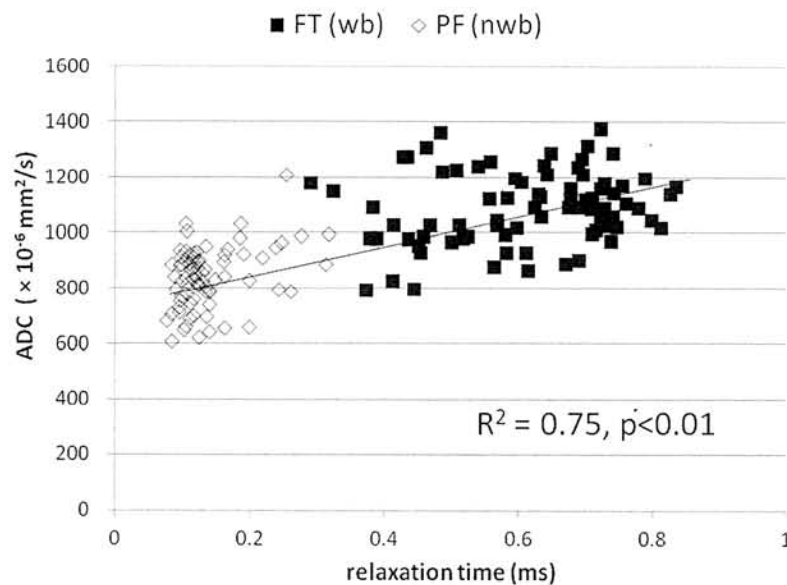
#### 4.4.5 Statistical analysis

The relationship between ADC and viscosity coefficient as well as that between ADC and relaxation time were assessed by means of correlation analysis. The correlation coefficients were assessed using a Pearson coefficient. Significant differences among the weight-bearing, non-weight-bearing, medial, and lateral regions were evaluated by

multiple comparison tests using one-way analysis of variance (ANOVA). Statistical significance was defined as  $p < 0.05$ . Statistical software (Statcel for Windows, OMS, Saitama, Japan) was used for all analyses.

## 4.5 Results

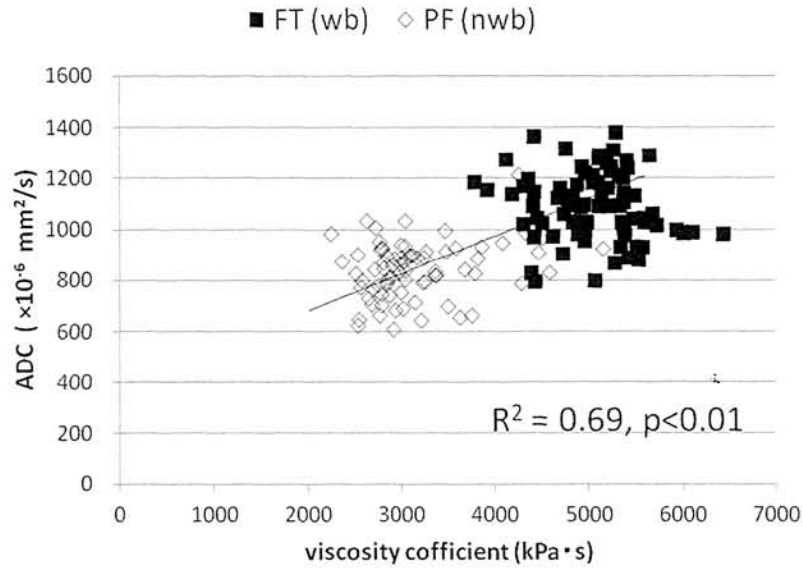
All porcine knees were visually healthy, with no blistering, ulceration, fissuring, or thinning of cartilage. ADC was correlated with relaxation time and viscosity coefficient ( $R^2 = 0.75$  and  $0.69$ , respectively,  $p < 0.01$ ) (Fig. 4-11, 4-12).



**Fig. 4-11** Correlation between ADC and relaxation time

A significant correlation between ADC and relaxation time was observed. The ADC of the weight-bearing region was significantly higher than that of the non-weight-bearing region.

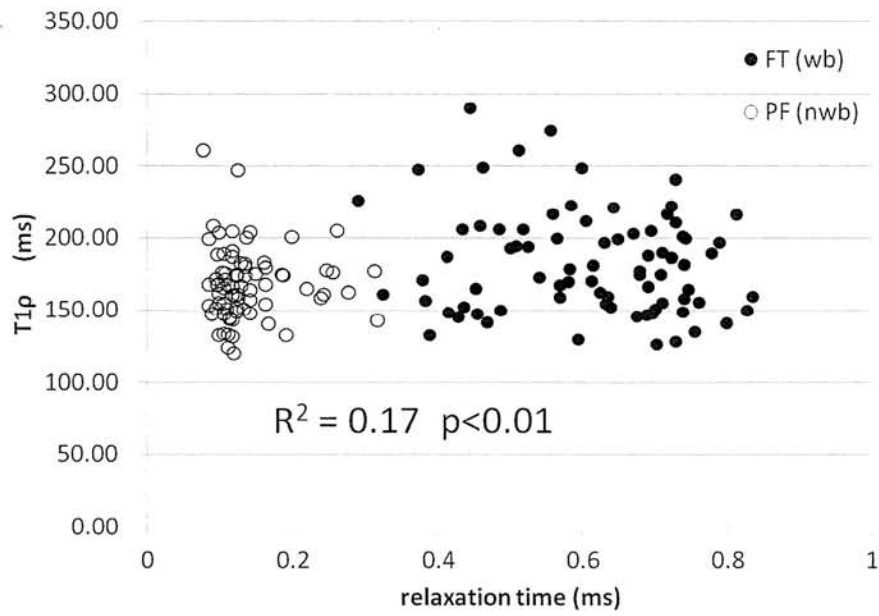




**Fig. 4-12** Correlation between ADC and viscosity coefficient

A significant correlation between ADC and viscosity coefficient was observed. The ADC and the viscosity coefficient in the weight bearing region were significantly higher than those in the non-weight bearing region.

On the other hand, T1 $\rho$  was poorly correlated with relaxation time and viscosity coefficient ( $R^2=0.17$  and  $0.26$ , respectively,  $p<0.01$ ) (**Fig. 4-13**). The mean relaxation time values in the weight-bearing and non-weight-bearing regions were  $0.61\pm0.17$  ms and  $0.14\pm0.08$  ms, respectively (**Table 4-2**). The mean viscosity coefficient values in weight-bearing and non-weight-bearing regions were  $5043\pm787$  kPa · s and  $3100\pm806$  kPa · s, respectively (**Table 4-2**).



**Fig. 4-13** Correlation between T1ρ and relaxation time

**Table 4-2** ADC, T1ρ and mechanical property of cartilage \*p<0.05

	FT	PF
ADC (mm <sup>2</sup> /s)	1088 ± 125*	835 ± 110*
T1ρ (ms)	182.97 ± 35.21*	168.01 ± 24.29*
viscosity coefficient (N•s/m <sup>2</sup> )	5.04 ± 0.79*	3.10 ± 0.81*
Relaxation time (ms)	0.61 ± 0.17*	0.14 ± 0.08*

Weight-bearing regions had significantly longer relaxation times and higher viscosity coefficient values than non-weight-bearing regions did ( $p < 0.05$ ). The mean ADC values in weight-bearing and non-weight-bearing regions were  $1087 \pm 125 \times 10^{-6} \text{ mm}^2/\text{s}$  and  $835 \pm 110 \times 10^{-6} \text{ mm}^2/\text{s}$ , respectively (**Table 4-2**). The mean T1 $\rho$  values in weight-bearing and non-weight-bearing regions were  $182.97 \pm 35.21 \text{ ms}$  and  $168.01 \pm 24.29 \text{ ms}$ , respectively (**Table 4-2**). All of these differences were statistically significant ( $p < 0.05$ ).

#### 4.6 Discussion

Cartilage plays a critical role in joint function, where it acts as a shock absorber during joint loading. This function is partly enabled by proteoglycan, which has a high negative charge and binds to water molecules, thereby generating the swelling pressure of cartilage [28]. This swelling pressure is counteracted by the tensile strength of cartilage, which is provided by a dense and regularly arranged collagen network [29-32]. Therefore, intermolecular interactions of both major components of cartilage with water molecules give cartilage its viscoelasticity, the characteristic that enables cartilage to act as a shock-absorber [15, 33]. The decrease in proteoglycans and disruption of the collagen network that occurs over time in degenerative cartilage leads

to a loss of viscoelasticity [16].

It has been suggested that differences in diffusivity as assessed by ADC may be due to differences in water mobility, which in turn is determined by the average pore size in the cartilage matrix [34-35]. The difference in diffusivity between tibiofemoral and patellofemoral cartilage, for example, might be due to differences in their inherent matrix structures and compositions. Indentation testing can directly evaluate the viscoelasticity of cartilage, and has been used in several studies to assess cartilage function in degenerative cartilage [36]. Recent studies have used arthroscopic indentation instruments for this purpose, but such indentation testing is somewhat invasive and should not be used as a routine clinical evaluation method. In comparison, MR imaging is less invasive and can be used more regularly for clinical evaluation. This study has uncovered significant correlations between ADC and relaxation time, as well as between ADC and viscosity coefficient, indicating that ADC can serve as an ideal measure of cartilage viscoelasticity.

There are several limitations of this study. First, only visually healthy cartilage specimens were recruited. Thus the usefulness of ADC as a means of assessing degenerative cartilage remains unknown. In addition, as biochemical and histological analysis were not performed, the usefulness of ADC as a quantitative measure of

cartilage degeneration is also unknown. These deficiencies constitute major weaknesses of this study.

As cartilage samples from several different regions of several different porcine knees were used, specimens with various cartilage matrix compositions were included. Therefore, the significant correlation observed between ADC and viscoelasticity lends support to the notion that ADC could be useful in the evaluation of degenerative cartilage as well. Further studies including knees with degenerative cartilage and incorporating biochemical and histological analysis are needed to confirm this. At present, however, it is unknown whether the results of the current study may be applied to the evaluation of repaired cartilage, degenerating cartilage, and/or mature knees.

A second limitation is that the indentation test was the only mechanical test performed on our cartilage samples. It has been shown that cartilage exhibits a much greater stiffness in tension than in compression, and that cartilage exhibits anisotropy in tension and compression. Further studies using other mechanical tests including tension tests may reveal a more detailed relationship between ADC and data on cartilage strength.

Third, we did not use any models of defective or degenerating cartilage in this

study, as we used only tissues from branded edible pigs, and as only immature porcine knees were included. It will be necessary to determine whether similar results can be obtained using repaired cartilage, degenerating cartilage, and/or mature knee cartilage in future studies before ADC is used clinically as a measure of cartilage viscoelasticity.

#### 4.7 Conclusion

A moderate correlation was observed between ADC and viscoelasticity in superficial articular cartilage. Both molecular diffusion and viscoelasticity were higher in weight-bearing than in non-weight-bearing regions of articular cartilage.

## **Chapter 5**      Evaluating relation between speed of sound and elasticity of the cartilage

### 5.1 Introduction

In previous studies, degeneration of cartilage was trying to be assessed by high frequency ultrasound by paying attention to the thickness, morphology, and surface roughness of cartilage [1-8], however, these tools cannot be used *in vivo*. In contrast, the pulse-echo method provides high-resolution images of articular and periarticular structures by real-time imaging display. The imaging assessment of the cartilage has been improved by the advent of the pulse-echo method with a wide dynamic range [9].

Evaluation of changes in the thickness and elasticity of cartilage is important for assessing its degeneration. Further, some studies have compared the measurement results of cartilage thickness using ultrasound with those obtained using optics, needles, microscopes *in vitro* [7-8].

In addition to morphology, conventional ultrasound elastography based on speckle tracking has been used as a noninvasive method for evaluating elasticity in several types of tissue, however, its application in cartilage is difficult, since cartilage

itself does not have any echo signals [10-11]. As an alternative, when the cartilage is assumed to be a solid with isotropic linear elasticity, the relationship among the SOS ( $c$ ), density ( $\rho$ ) Young's modulus ( $E$ ), and Poisson's ratio ( $\nu$ ) is expressed as follows:

$$c = \sqrt{E(1-\nu) / \rho(1+\nu)(1-2\nu)} \quad (1)$$

Therefore, the elasticity of cartilage can be assumed by the SOS in it which is calculated from the thickness of a given cartilage and the propagation time of the ultrasound within it [8, 12]

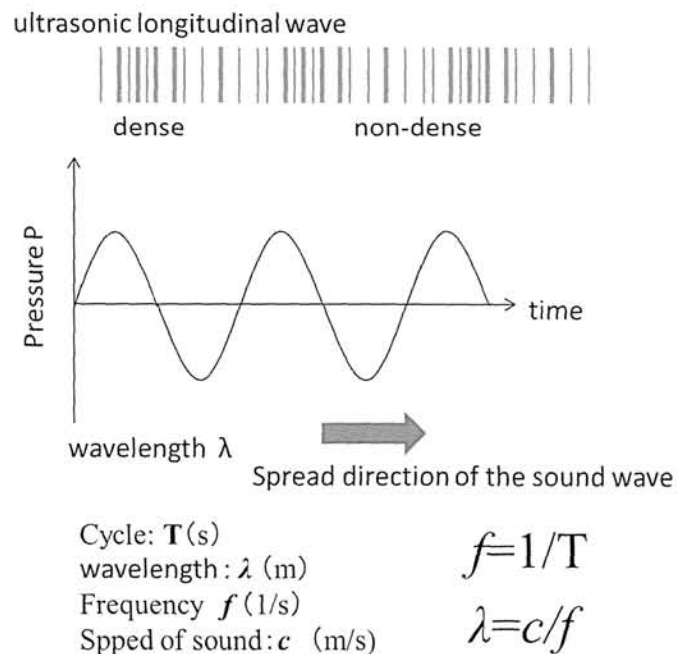
In this study, the accuracy of our proposing method of combination of MRI and ultrasound via the pulse-echo methods (combination method) in the assessment of SOS of cartilage that should correlate with the severity of its degeneration is evaluated. In the imaging of the cartilage by the pulse-echo method, longitudinal wave of the ultrasound was used. In the current study, preciseness of MR measurement of objects' thicknesses and accuracy of SOS provided by the combined method were first evaluated in agar phantom followed by in porcine knee cartilage. The applicability of the combined method to humans was also examined.



## 5.2 Theory supporting the speed of sound measurements

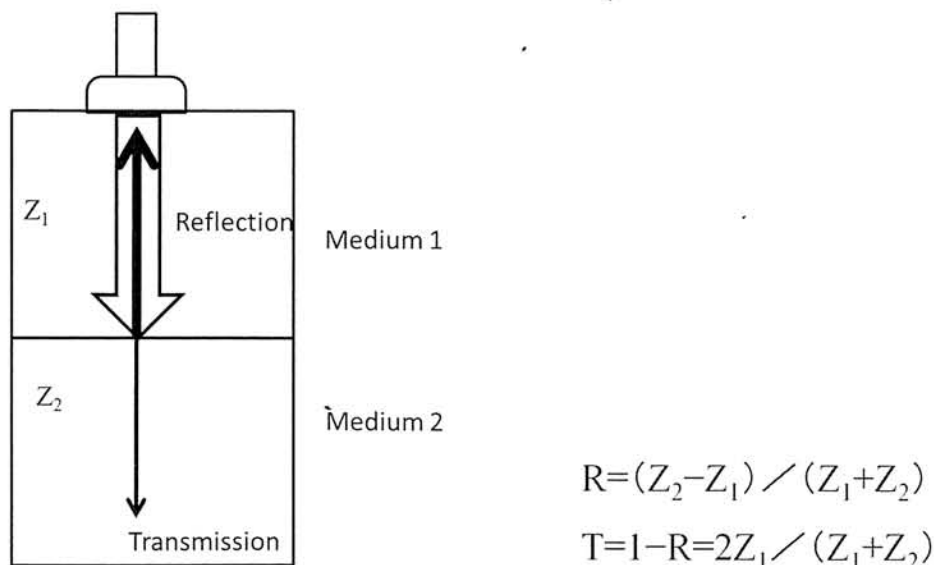
### 5.2.1 Basic ultrasound

Ultrasound is simply sound waves, and some physical properties are dependent on the frequency. Sound consists of waves of compression and decompression of the transmitting medium (e.g. air or water), traveling at a fixed velocity. Sound is an example of a longitudinal wave oscillating back and forth in the direction the sound wave travels, thus consisting of successive zones of compression and rarefaction. Transverse waves are oscillations in the transverse direction of the propagation (**Fig. 5-1**).



**Fig. 5-1** Longitudinal compression wave and transverse wave

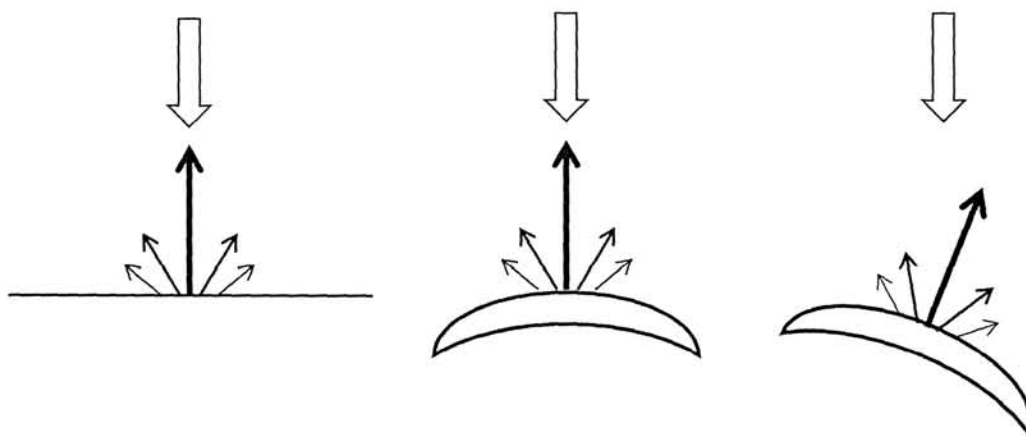
Basically, all ultrasound imaging is performed by emitting a pulse, which is partly reflected from a boundary between two tissue structures, and partially transmitted (**Fig. 5-2**). The reflection depends on the difference in impedance of the two tissues. Basic imaging by ultrasound does only use the amplitude information in the reflected signal. One pulse is emitted, the reflected signal, however, is sampled more or less continuously (actually multiple times). As the velocity of sound in tissue is fairly constant, the time between the emission of a pulse and the reception of a reflected signal is dependent on the distance; i.e. the depth of the reflecting structure. The reflected pulses are thus sampled at multiple time intervals (multiple range gating), corresponding to multiple depths, and displayed in the image as depth (**Fig. 5-2**).



**Fig. 5-2** Reflection and transmission

The amplitude of the reflected signal, is not only dependent on the reflection coefficient. The direction of the reflected signal is also important.

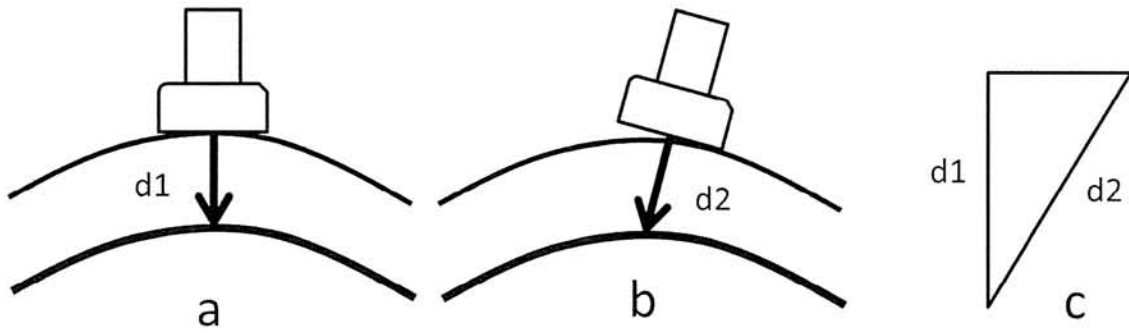
- An irregular scatterer will reflect only a portion back to the probe.
- A more regular scatterer will reflect more if the reflecting surfaces are perpendicular to the ultrasound beam.



**Fig. 5-3** Scatter and reflecting surfaces

#### 5.2.2 Incidence angle and the distance

In a thickness measurement, the distance when a beam was incident perpendicularly becomes the minimum. Oblique incidence causes artifacts by scatter.



**Fig. 5-4** Incidence angle and the distance

Perpendicularly incident (a), oblique-incidence (b), distance (c).

### 5.2.3 The transmission method measurement of speed of sound (SOS)

The transmission method was implemented using planar non-focusing transducers with a center frequency of 5 MHz and an aperture diameter of 0.25 inch (124-340, GE Inspection Technologies, Wichita, KS, USA) by noncontact at a distance of 30 mm. Each agar phantom was placed in a laboratory dish filled with saline with through-transmission geometry, and the propagation time was measured without and with the agar phantom at room temperature (18.4°C) (**Fig. 5-5a, b**). Measuring and averaging the time between multiple echoes yields highly precise propagation times (**Fig. 5-5c**).

SOS was measured according to the following formulae, where  $l_1$  is the distance between the transducer and the agar phantom,  $l_2$  is the specimen thickness,  $c_0$

is the SOS of saline, and  $t_0$  and  $t_1$  are one-way propagation times without and with the agar gel phantom, respectively.

$$\left\{ \begin{array}{l} l = l_1 + l_2 \\ t_1 = l_2/c + l_1/c_0 \\ t_0 = l/c_0 = l_1/c_0 + l_2/c_0 \end{array} \right. \quad \begin{array}{l} (1) \\ (2) \\ (3) \end{array}$$

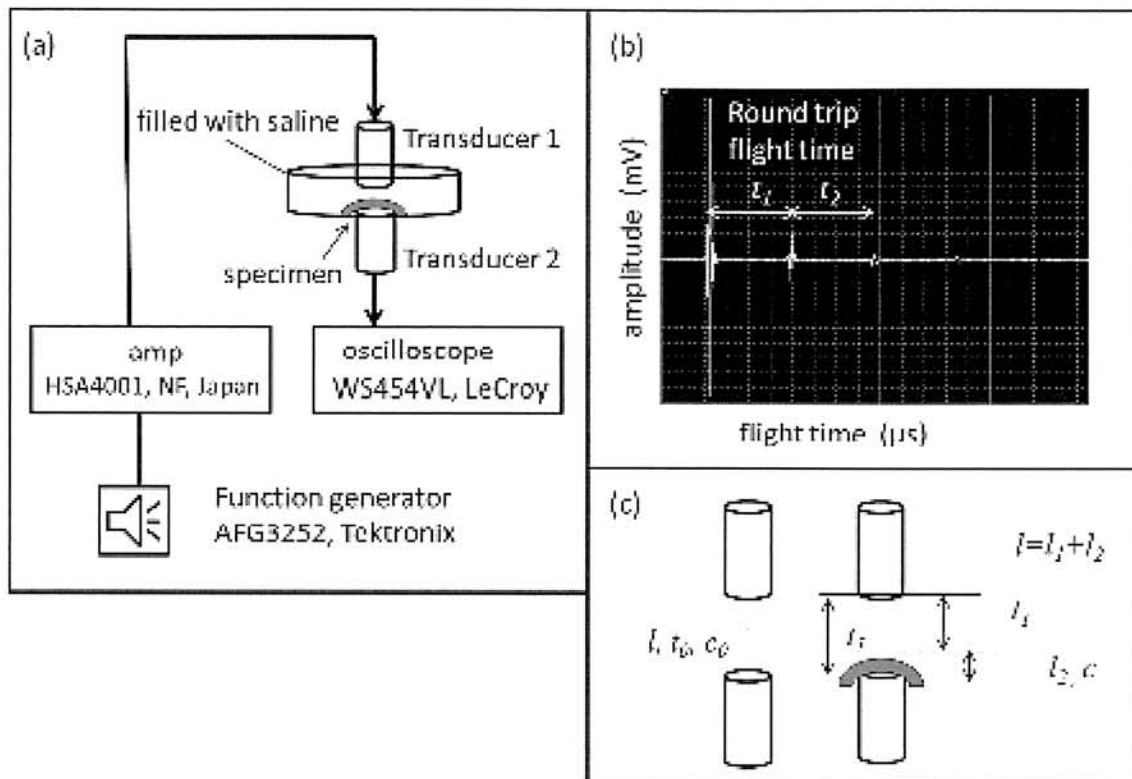
The difference in propagation times with and without the agar phantom is expressed as follows:

$$\begin{aligned} t_1 - t_0 &= (l_2/c + l_1/c_0) - (l_1/c_0 + l_2/c_0) \\ &= l_2/c - l_2/c_0 \\ &= l_2 (1/c - 1/c_0) \end{aligned} \quad (4)$$

Hence, the SOS of the agar phantom can be calculated as follows:

$$c = l_2 / ((t_1 - t_0)/l_2 + l_1/c_0) \quad (5)$$

The round-trip propagation time of each phantom was measured using an oscilloscope. The actual SOS was calculated from the propagation time using Eq. (5).



**Fig. 5-5** cartilaginous speed of sound measurement by transmission method

A cartilage specimen is placed in a laboratory dish filled with saline. An ultrasonic wave entering from transducer 1 penetrates the specimen and is received by transducer 2 (a). The propagation time of each round trip is measured using an oscilloscope (b). Measuring and averaging the time between multi-echoes yields high-precision measurements of propagation time ( $t$ ).  $t = (t_1 + t_2) / 2$ ,  $t_1$ : 1st- 2nd wave,  $t_2$ : 2nd-3rd wave. Schematic illustration of the method for measuring speed of sound of specimens (c). Regardless of whether the specimen is present, speed of sound is measured from the same distance.

#### 5.2.4 The SOS measurement by combination method

Distance of two points on ultrasound imaging using pulse-echo method is calculated from the flight time (TOF) of the ultrasound between the two points and the

specifically fixed SOS as Eq. (2) In Japanese ultrasound machines, the fixed SOS is determined as 1530 m/s by Japanese Industrial Standards.

$$\text{Distance}_{(\text{pulse-echo method})} = \text{SOS}_{(\text{fixed})} \times \text{TOF} \quad (6)$$

*Where TOF is flight time of the ultrasound between the two points*

Since true distance is calculated by true SOS as Eq. (3) and Eq. (4) is obtained from Eq. (2) and Eq. (3).

$$\text{Distance}_{(\text{true})} = \text{SOS}_{(\text{true})} \times \text{TOF} \quad (7)$$

$$\text{SOS}_{(\text{true})} / \text{SOS}_{(\text{fixed})} = \text{Distance}_{(\text{true})} / \text{Distance}_{(\text{pulse-echo method})} \quad (8)$$

Therefore, true SOS; which we would like to obtain for the assessment of degeneration of cartilage is calculated as below.


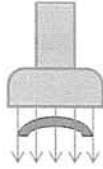

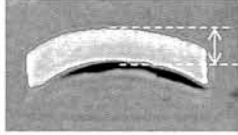
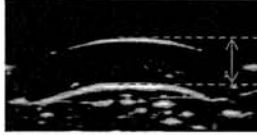
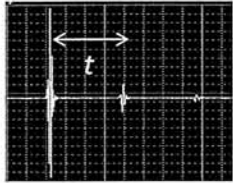
$$\text{SOS}_{(\text{true})} = \text{SOS}_{(\text{fixed})} \times \text{Thickness}_{(\text{true})} / \text{Thickness}_{(\text{pulse-echo method})} \quad (9)$$

Then, when the thickness of the cartilage is accurately measure by MRI, true SOS of the cartilage is calculated as below.

$$\text{SOS}_{(\text{cartilage})} = \text{SOS}_{(\text{fixed})} \times \text{thickness}_{(\text{MRI})} / \text{thickness}_{(\text{pulse-echo method})} \quad (10)$$

Where  $\text{SOS}_{(\text{cartilage})}$  is true SOS of cartilage,  $\text{SOS}_{(\text{fix})}$  is 1530 m/s (our device),  $\text{thickness}_{(\text{MRI})}$  and  $\text{thickness}_{(\text{pulse-echo method})}$  are measured thickness of cartilage by MRI and ultrasound via pulse-echo method.

Table 5-1 Summary of ex vivo measurement

	MRI	Pulse echo	Transducers
Method			
Measured Result	 $d_{MR}$	 $d_{US}$	
	$d_{MR} \doteq d$	$d_{pulse\ echo} = d \times 1530 / c$	$d / 2 = c \times t$
Remarks	$d$ : Real thickness $c$ : Speed of sound $t$ : Roundtrip flight time		
	$c > 1530, d_{MRI} > d_{pulse\ echo}$		
Calculate	$c = 1530 \times d_{MRI} / d_{pulse\ echo}$		$c = 2d / t$

## 5.3 Materials and Methods

### 5.3.1 Specimen preparation

Three-percent (w/v) agar phantoms ( $n = 10$ ), approximately 5 mm in thickness, were made from agar powder (010-15815, Wako Pure Chemical Industries, Osaka, Japan) dissolved in heated deionized water, with glycerin added in concentrations ranging from 10% to 60% (w/v) (075-00611, Wako Pure Chemical Industries, Osaka, Japan). The SOS in agar phantoms varies according to the concentration of glycerin [13], and those made for this study incorporated different concentrations of glycerin, in steps of



five percent.

Fresh porcine knee joints ( $n = 6$ ) were obtained from a local abattoir (ZEN-NOH Central Research Institute for Feed and Livestock, Ibaraki, Japan). In each specimen, disks 12 mm in diameter (total,  $n = 24$ ) were harvested from four sites on the medial and lateral femoral condyles. The subchondral bone was removed from each specimen using a punch and a razor [14]. All specimens were encased in agar after the transmission method measurement, and next, MRI and pulse-echo ultrasound measurements were performed.

### 5.3.2 MRI imaging

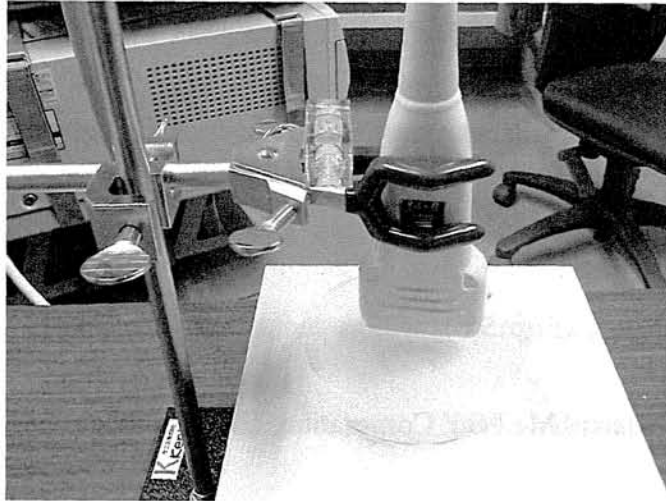
MRI was performed using a 3.0T whole-body clinical scanner (InteraAchieva; Philips Medical Systems, Best, Netherlands) with a 4-ch sensitivity encoding (SENSE) wrist coil employing a parallel imaging technique. Morphological isotropic voxel images were acquired using a three-dimensional (3D) fast-field echo (FFE) sequence with the following parameters: repetition time (TR)/echo time (TE1/TE2), 19/7.0/13.3 ms; field of view (FOV),  $80 \times 80$  mm; scanned matrix,  $512 \times 512$  (acquired matrix:  $256 \times 256$ ); voxel size,  $0.3 \text{ mm}^3$ ; and number of excitations, 1. Fat suppression was achieved using ProSet (total scan duration: 309 s). Outline extraction for measuring the cartilage

thickness was carried out manually.

### 5.3.3 Thickness measurements of specimens

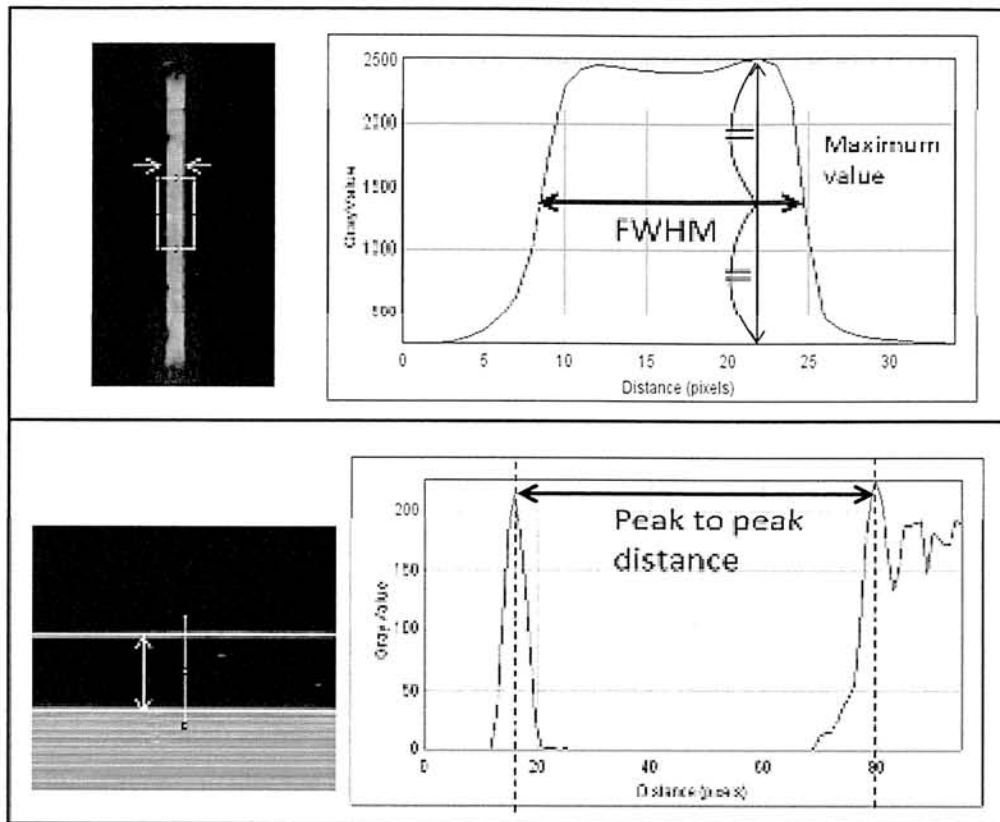
The accuracy of cartilage thickness measurements was evaluated using agar phantoms and porcine knee cartilage specimens using the following modalities: pulse-echo ultrasound measurements (**Fig. 5-6**), with a center frequency of 10 MHz with fixed SOS (EUB-7500; Hitachi Medical Corporation, Tokyo, Japan); MRI as described above; a non-contact laser (spot diameter, 70  $\mu\text{m}$ ; LK-G35, LKGD500, Keyence, Japan); and a digital caliper (Mitsutoyo, Kanagawa, Japan). In the pulse-echo ultrasound measurements, thickness was obtained using the peak-to-peak distance of profiles (**Fig.5-7a**). In MRI measurements of thickness, agar phantom thicknesses were obtained using the full width at half maximum (FWHM, **Fig. 5-7b**), and the thicknesses of cartilage specimens were obtained from the peak-to-peak distance of profiles, using manual outline extraction. All thickness measurements were processed using Image J software (version 1.45, National Institutes of Health, Bethesda, Maryland, USA). Since the repetitive accuracy of laser measurements is on the order of 0.05  $\mu\text{m}$ , the thickness measurements obtained by the laser device were considered gold standard values. Each measurement was performed five times and mean values of

these measurements were used in this study.



**Fig. 5-6** Image of the SOS measurement of the agar gel phantom by pulse echo method

The put laboratory dish of the sample is filled with a saline. The probe is fixed to the laboratory dish perpendicularly and is scanned. The horizontal level of the probe is confirmed with a level. The central domain of a sample is scanned from in every direction.



**Fig. 5-7** Schema of thickness measurement profile

Thickness measurement profile of agar gel phantom using the profile peak-to-peak thickness measurement for the pulse-echo method (a), and the full width at half maximum (FWHM) value for MRI (b). The MRI image was reconstructed using a 1024 matrix, and the mean value of the thickness in the region of interest was measured in three dimensions, whereas for the pulse-echo method, the thickness was measured in two dimensions.

#### 5.3.4 SOS measurements in cartilage specimens

The SOS in cartilage specimens was measured using the combination of pulse-echo ultrasound and MRI, as described above, and also transmission ultrasound. The SOS

values obtained using transmission ultrasound measurements alone were compared with those obtained via the combined method, using the agar phantoms and porcine knee cartilage specimens. The transmission ultrasound method was implemented using planar non-focusing transducers with a center frequency of 5 MHz and an aperture diameter of 0.25 inch (124-340, GE Inspection Technologies, Wichita, KS, USA), using a noncontact method [15] at room temperature (18.4°C). The high accuracy of the TOF obtained from the oscilloscope was possible by averaging the multiple pulses. Each measurement was performed five times, with mean values used as data.

### 5.3.5 Statistics

Statistical analysis was performed using the Wilcoxon signed-ranks test. Statistical significance was defined as  $p < 0.05$ . Statistical software (Statview, version 5; SAS Institute, Cary, NC, USA) was used for all analyses.

## 5.4 Results

### 5.4.1 Thickness measurements of specimens

The mean thicknesses of the agar phantoms obtained using MRI and laser measurements were  $5.41 \pm 0.49$  and  $5.39 \pm 0.53$  mm, respectively. Thus, there was no significant difference between MRI and laser measurements ( $p=0.64$ ). The mean thicknesses of porcine knee cartilage specimens obtained using MRI and digital caliper measurements were  $2.96 \pm 0.95$  and  $3.03 \pm 0.96$  mm, respectively ( $R^2= 0.92$ ). There was no significant difference between these thicknesses ( $p=0.60$ ).

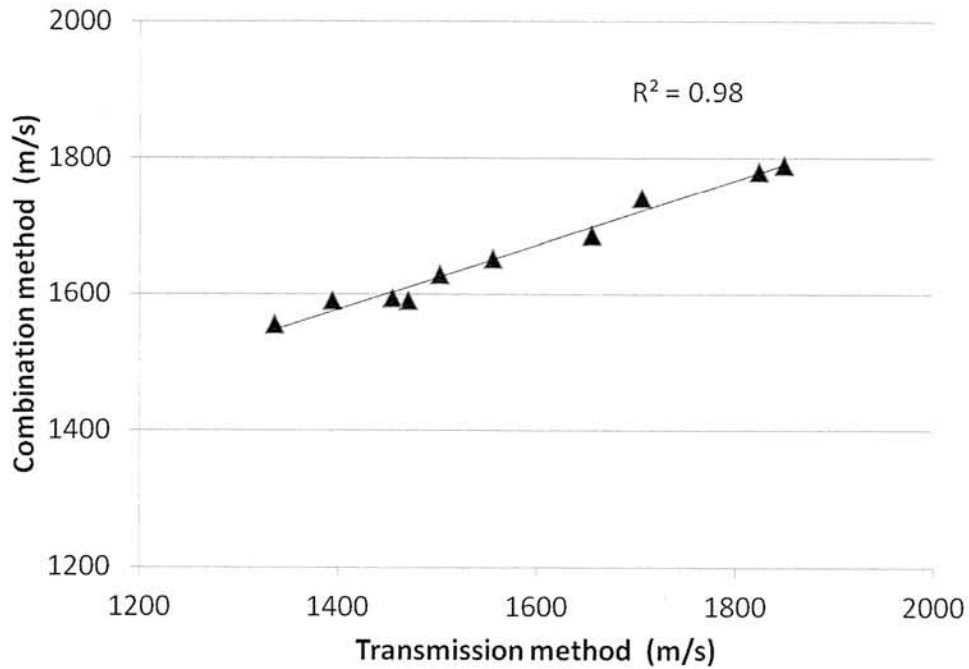
### 5.4.2 Comparison of SOS using transmission method and combination method

The SOS in agar phantoms without glycerin was measured using transmission ultrasound and showed a constant value (approximately 1475 m/s, at 18.4°C). When the SOS in agar phantoms that included different concentrations of glycerin was measured, the SOS values were increased with increasing glycerin concentrations. The measured SOS values increased by 36.38 m/s per 5 % of added glycerin, when measured with

transmission ultrasound, and increased by an 35.67 m/s per 5 % of added glycerin when measured using the combined measurement method of MRI and pulse-echo ultrasound.

**Fig. 5-8** shows the relation between the SOS measured in agar phantoms that include various concentrations of glycerin for the pulse-echo ultrasound and transmission ultrasound methods. A significant linear correlation was observed between the results based on the combined method and those based on transmission ultrasound alone ( $R^2 = 0.98, p < 0.05$ ).

The mean SOS in the porcine knee cartilage specimens was calculated for ultrasound transmission method with caliper and for the combined method as  $1629 \pm 74$  and  $1575 \pm 119$  m/s, respectively. The SOS values obtained by these two methods showed a significant correlation ( $R^2 = 0.92, p < 0.05$ ).



**Fig. 5-8** Correlation of agar phantom's SOS between transmission method and combination method.

Pulse-echo method and transmission method shows strong correlation, and the coefficient of correlation is 0.96. The high accuracy of the combination method was confirmed.

## 5.5 Discussion

The present study demonstrated the accuracy of our proposed method of combined MRI and pulse-echo ultrasound measurements for the assessment of SOS in cartilage. The accuracy of SOS measurements using the combined method depends on the accuracy of the cartilage thickness measurements. It is known that pulse-echo ultrasound provides



very high spatial resolution. Although Eckstein et al. reported the underestimation of cartilage thickness measurements when using a 1.5T MRI system, and suggested that the low SNR and low spatial resolution of the MR images were possible reasons for the inaccuracies [16-17], our thickness measurements of agar phantoms using a 3T MRI system indicated that the thickness of these objects could be accurately measured, with an error of less than a single pixel. The smallest isotropic voxel size of MR images is typically 0.6 mm in clinical use, but improvements in compression sensing technology is expected to lower this limit in the near future.

The SOS measurements using the combined method and the ultrasound transmission method showed a high correlation in agar phantoms. There was no significant difference in measurements using these two methods, and measurements using the combined method were correctly obtained. Furthermore, the SOS in porcine knee cartilage specimens measured by the combined method in our study was similar to that of previous studies [5, 8].

The cartilage thickness measurement necessary for calculations of SOS in the tissue were based on morphological images, but the obtained SOS values only provide local information. Using two modalities to obtain the SOS is a demerit but there is also an advantage, namely that of enabling measurements of elasticity in *in vivo* tissue, which

was previously assumed to be impossible. In any case, when using the two measurement modalities, thickness measurements of congruent areas can be obtained by using Real-time Virtual Sonography (RVS). Thus, the SOS measurements obtained by the combined method allow the elasticity in living tissue such as cartilage to be evaluated, which cannot be done using conventional elastography. For instance, our method may be useful for follow-up examinations in osteoarthritis (OA) patients who have received grafts of regenerated cartilage.

## 5.6 Conclusions

The present study demonstrated the accuracy of the proposed measurement method that combines MRI and pulse-echo ultrasound measurements to assess the SOS in cartilage. The use of this method as a new non-invasive diagnostic tool may be expected.

## **Chapter 6**      Comparison of the speed of sound and T2 relaxation time of the cartilage in the assessment of its degenerative change

### 6.1 Introduction

The speed of sound (SOS) in tissue varies according to its pathological condition [1-3]. Kiviranta et al. [4] investigated the SOS in cartilage and reported that the more samples were degenerated, the slower was the SOS in them, and the relationship between tissue stiffness and the SOS in tissue was demonstrated via indent tests which agree with theoretical equation. Therefore, an accurate method for measuring SOS in cartilage would be valuable for diagnosing osteoarthritis (OA), especially if it could be applied to *in vivo* measurements. The assessment of cartilage with ultrasound imaging has been improved by the advent of the pulse-echo method that has a wide dynamic range [5]. In this study, we evaluated the accuracy of our proposed method of combining magnetic resonance imaging (MRI) with ultrasound to assess the SOS in cartilage, which is thought to correlate with the severity of degeneration caused by OA. In current study, the accuracy of MR measurements of objects' thicknesses which is

key step to obtain SOS was first evaluated in agar phantoms. The applicability of the combined method for *in vivo* measurements was then examined.

## 6.2 Materials and Methods

### 6.2.1 Subjects

This study was approved by the Committee for Human Research at our institution, and prior informed consent was obtained from all subjects. Fourteen volunteers (eight females, six males, mean age 37.9 years; rang 22-51 years) underwent MRI and ultrasound via the pulse-echo method with a center frequency of 10 MHz with fixed SOS (EUB-7500; Hitachi Medical Corporation, Tokyo, Japan).

### 6.2.2 MR imaging

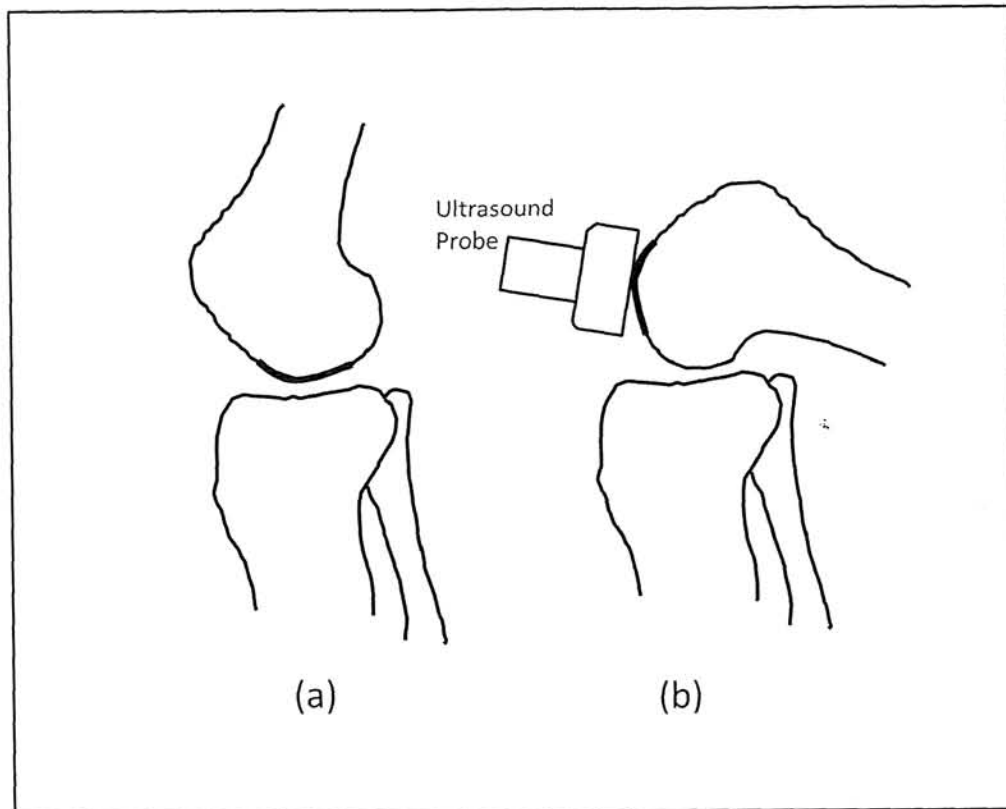
MRI was performed by the above-described scanner with the 8-ch SENSE knee coil, with isotropic images acquired using the 3D-FFE sequence described above. The possibility of OA was evaluated in each subject using T2 relaxation times. T2 relaxation time is used to identify joint changes associated with OA that indicates the properties of the collagen fibril network [6-7]. T2-mapping was acquired using a multi-slice

multi-echo two-dimensional T2 mapping sequence with the following parameters: TR/TE 2000/40,60,80 ms; FOV  $160 \times 160$  mm; scanned matrix,  $320 \times 320$ ; 3.0 mm section thickness; 0.3 mm spacing; one excitation. Sagittal MR images were acquired along a plane perpendicular to a line passing through both the medial femoral and lateral femoral condyles. The T2-map was reconstructed by fitting the image intensity pixel-by-pixel to the equation  $S_{(TE)} = \exp(-TE/T2)$ . The 3D-FFE sagittal image was reconstructed from a section perpendicular to the cartilage at the center of the femoral condyle so that cartilage thickness could be accurately measured. Cartilage thicknesses were always measured perpendicularly to the structure, to minimize measurement error [8].

### 6.2.3 Problem of applying the pulse-echo method

The cartilage thickness of a weight-bearing region cannot be measured by the pulse-echo method with the same posture as MRI. MR examination was performed with the knee position at mild flexion, since MR imaging of the knee at maximum flexion is impossible because of a relative small MR bore size of 600 mm in diameter. On the other hand, pulse-echo method was performed with the knee position of maximum flexion, since the cartilage of the knee is observed only at maximum flexion on

pulse-echo method (**Fig. 6-1**). It is difficult to identify the same part in two different postures. In pulse-echo method, measurements of the cartilage were always performed trying to measure the exact same position to the MR measurement with referring to the MR images of the knee including surrounding structures. Agreement of the measuring points between the two methods was also investigated using one volunteer. MR imaging of the knee in the mild flexed position and the maximum flexed position was performed on a single young healthy volunteer (female, age 25) using the same scanner described above with a two-element SENSE Flex coil employing a parallel imaging technique; morphological isotropic images were acquired using a 3D-FFE sequence with the same parameters described above.



**Fig. 6-1** Schema of flexure of the patella and the knee

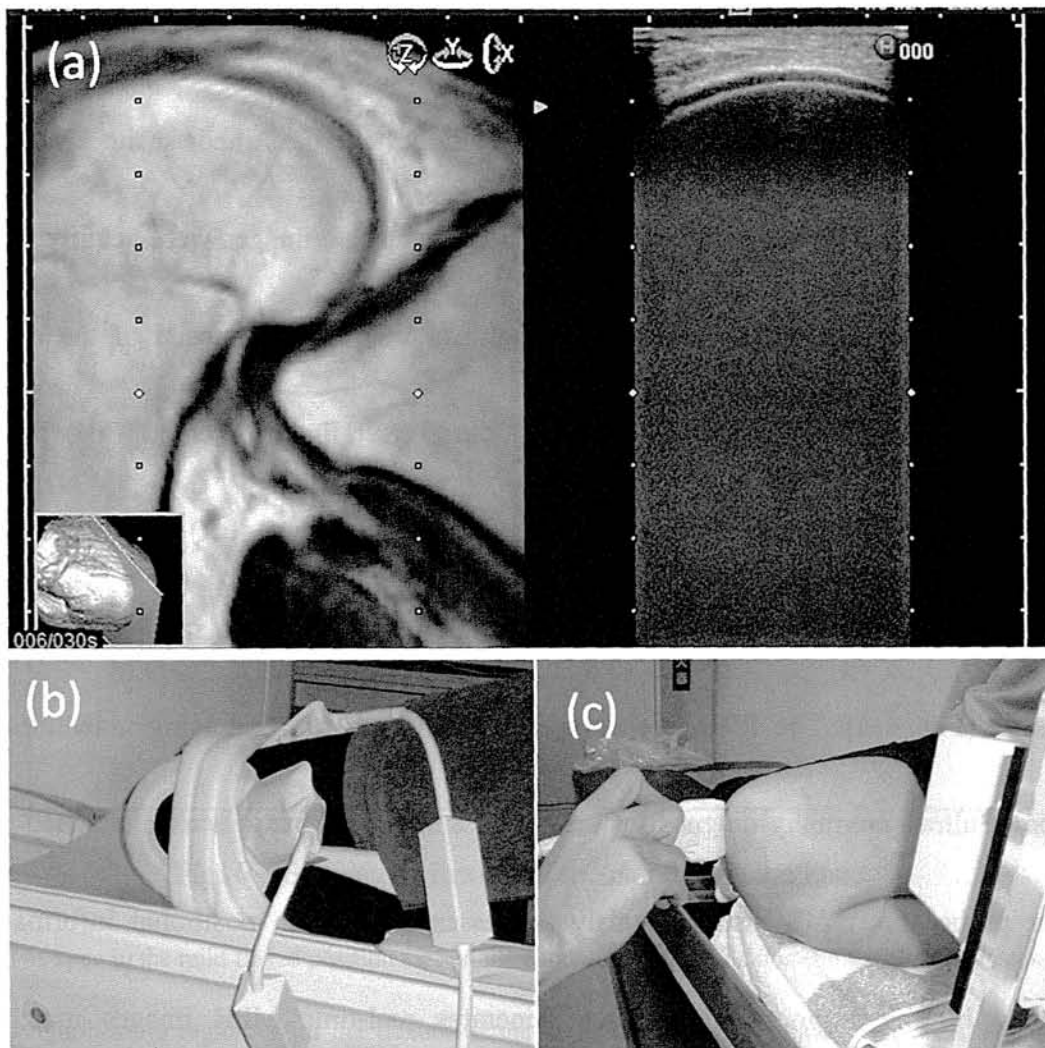
The knee in the mild flexed position (a) and the maximum flexed position (b). Red line indicates the weight-bearing region. With the flexure of the knee, the patella moves and the weight-bearing region appears.

#### 6.2.4 Applying the real-time virtual sonography (RVS)

When making ultrasound measurements of knee cartilage *in vivo*, we aimed to use the same position as that used in the MR measurement, by referring to the MR image of the knee, including surrounding structures. The congruency of the points measured with the two methods was investigated using a volunteer, as follows. MRI of the knee of a young

healthy volunteer (female, 25 years of age) was performed with the knee in positions of mild flexure and maximum flexure, using the above-described scanner with a two-element SENSE Flex coil, and morphological isotropic images were acquired. The system used for Real-time Virtual Sonography (RVS) was composed of the digital ultrasound EUB-8500 device and Workstation RVS (Hitachi Medico Co., Tokyo, Japan), which generates real-time multiplanar reconstruction (MPR) images [9]. The degree of congruity between the points measured using these two methods was then assessed (**Fig. 6-6**). The RVS, a revolutionary real-time MPR imaging machine that supports ultrasonography diagnosis, consists of a small magnetic sensor attached to a linear probe. The RVS instantaneously processes changes in positional information detected by the magnetic sensor and generates real-time MPR images matching cross-sectional images of the cartilage captured by the probe (**Fig. 6-3**).





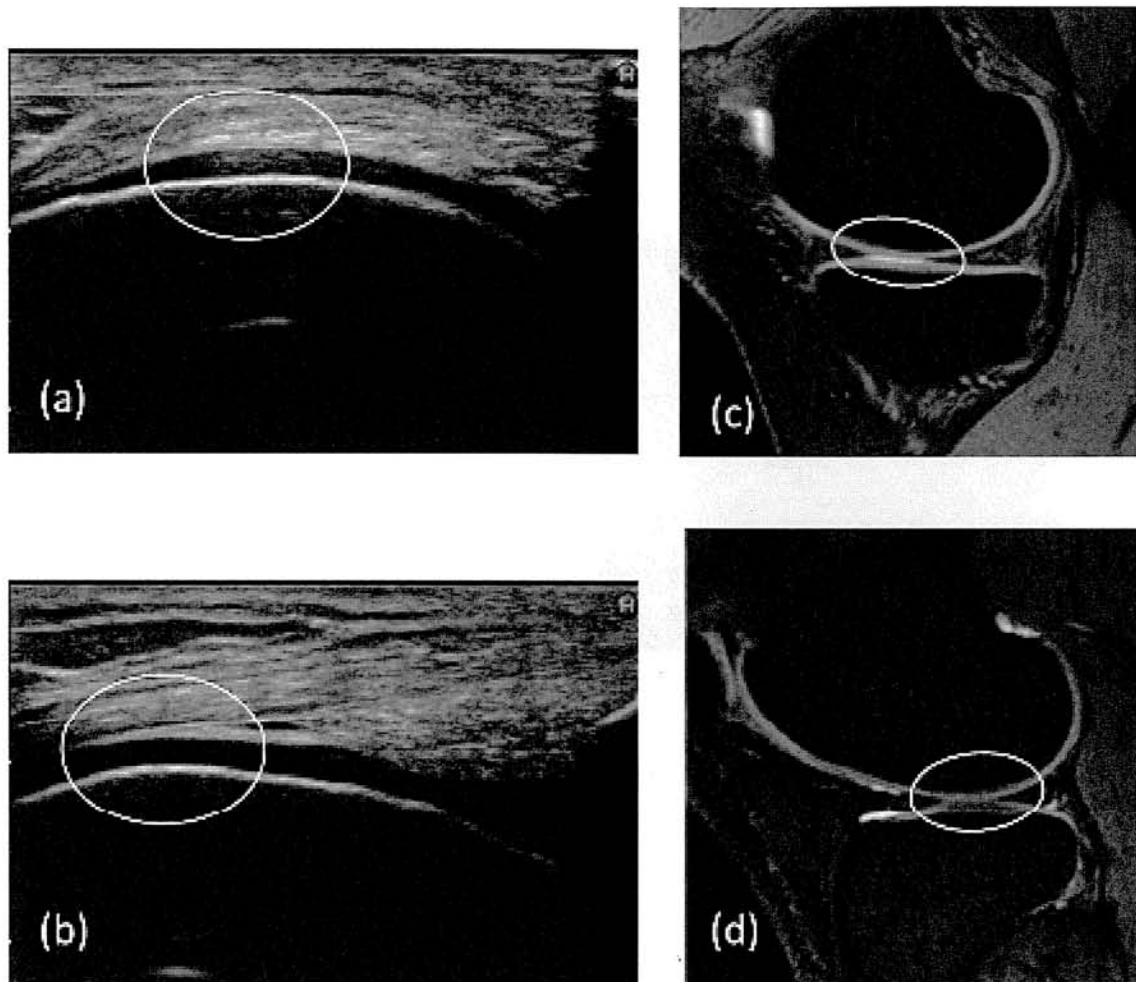
**Fig. 6-3** Image of the real-time virtual sonography (RVS)

Confirmation of congruity between regions measured by pulse-echo ultrasound and MRI methods.

Measurement point congruity was confirmed using real-time virtual sonography (RVS). RVS images were displayed on a monitor as a 3D MR image in the left half and a real-time image of the area being scanned in the right half (a). MRI of a knee in mild flexure carried out beforehand (b), and ultrasound in RVS (c).

The positions of the medial and lateral condyles were checked. **Fig. 6-4** shows the

medial (a,c) and lateral (b,d) condyle area confirmed by RVS.



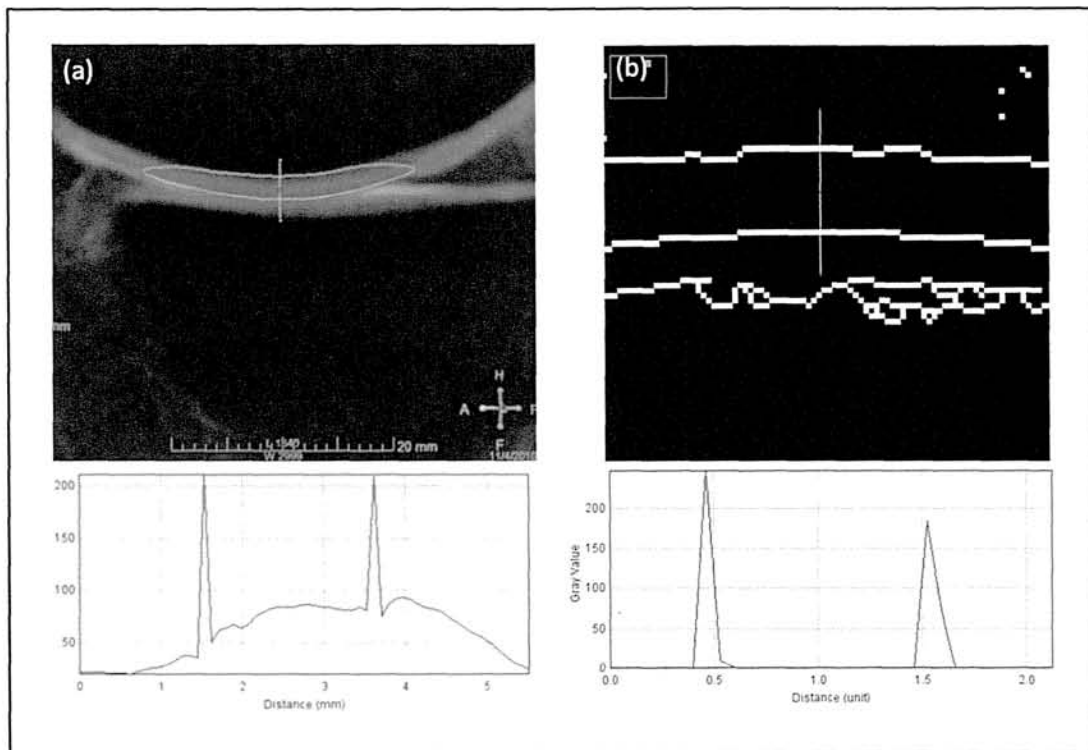
**Fig. 6-4** Position relations of the ultrasound image and the MR image

The weight-bearing region of the medial condyle is depicted slightly ahead of the center (a,c), and the weight-bearing region of the lateral condyle is depicted slightly behind the center (b,d).

#### 6.2.5 Definition of the cartilage thickness

Cartilage thickness in MRI images was measured by manual outline extraction, and that in ultrasound images was measured using binary images [10-11]. In both methods,

peak-to-peak thickness measurement profile using Image J software was performed (Fig. 6-5).



**Fig. 6-5** Definition of the cartilage thickness

Thickness measurement profile of the knee using peak-to-peak thickness measurements for MRI (a) and pulse-echo ultrasound (b). Cartilage thickness in MRI images was measured by manual outline extraction, and that in ultrasound images was measured using binary images.

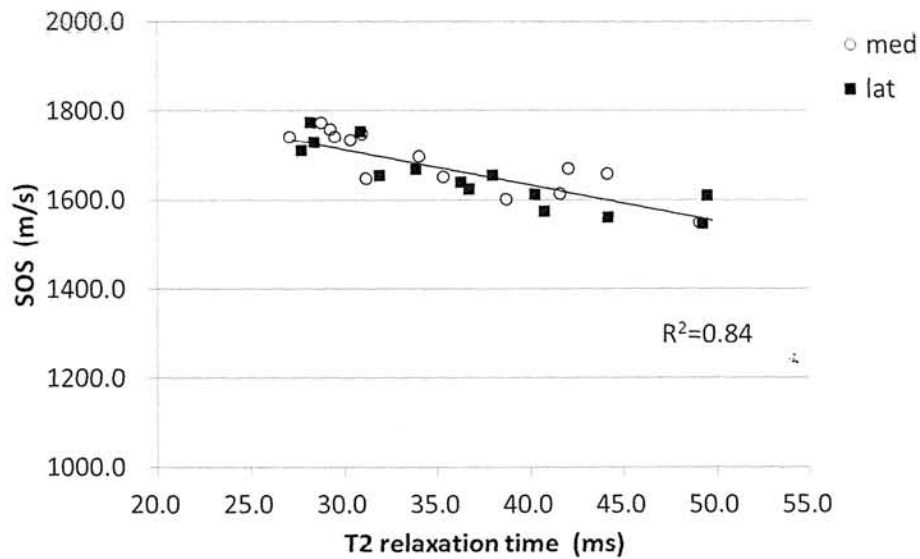
#### 6.2.6 Statistics

Statistical analysis was performed using the Wilcoxon signed-ranks test and Spearman's rank correlation coefficient. Statistical significance was defined as  $p < 0.05$ .

Statistical software (Statview version 5; SAS Institute, Cary, NC, USA) was used for all analyses.

### 6.3 Results

The mean T2 relaxation times when acquiring MRI data of medial and lateral condyles were  $35.1 \pm 6.8$  and  $36.8 \pm 7.3$  ms, respectively. The mean thicknesses of the medial and lateral condyles obtained by ultrasound were  $1.63 \pm 0.36$  and  $1.65 \pm 0.37$  mm, respectively. The mean thicknesses of the medial and lateral condyles obtained by MRI were  $1.80 \pm 0.39$  and  $1.82 \pm 0.41$  mm, respectively. Using these data, the SOS in cartilage at the medial and lateral femoral condyles was calculated for the combined method, using Eq. (2), with results of  $1684 \pm 68$  and  $1650 \pm 70$  m/s, respectively. A negative correlation was observed between measured SOS values and T2 relaxation times in knee cartilage measurements ( $R^2 = 0.84$ , **Fig. 6-7**). There were no significant differences between medial and lateral condyles ( $p=0.99$ ).



**Fig. 6-7** Correlation between SOS and T2

SOS and T2 relaxation time showed negative correlation ( $R^2= 0.84$ ). SOS values were lower in higher T2 relaxation time.

## 6.4 Discussion

The present study demonstrated the method of using combined MRI and ultrasound measurements to assess the degree of cartilage degeneration according to the SOS in the cartilage, and its applicability was evaluated using human volunteers.

The accuracy of SOS measurements depends on the accuracy of the cartilage thickness measurements. Previously, Eckstein et al. reported the underestimation of

cartilage thickness measurements when using a 1.5T MR system, and suggested that the low SNR and low spatial resolution of the MR images were possible reasons for the inaccuracies [12-13]. In our thickness measurement tests using agar phantoms, the 3T MRI system was able to measure the precise thickness of objects, with an error of less than one pixel. The smallest isotropic voxel size of MR images is typically 0.6 mm in clinical use, but improvements in compression sensing technology is expected to lower this limit in the near future.

Concerning measurements in human subjects, there was a problem of ensuring congruence between the ultrasound and MR measurement sites. However, the RVS study indicated that knee cartilage sites viewed with ultrasound with the knee at maximum flexion corresponded closely with the weight-bearing sites of the cartilage on MRI. In each case, the choice of precise ultrasound measurement points was aided by referring to MR images of the particular knee, including the surrounding structures such as the patella, musculature, and ligaments. Minimum thickness measurements were carried out with ultrasound pulses applied orthogonally to the cartilage, and measurements were recorded on video so that the appropriate orientation could be confirmed. SOS values observed in our study were similar to those of previous studies (**Table 6-1**) [1, 14-15]. Since the minimum value of the cartilage thickness obtained

from ultrasound image will be obtained accurately by providing graphical user interface, the problems which depend on repeatability and measurement accuracy is improved.

T2 relaxation times reflect collagen fibril network integrity with particular sensitivity [16], and longer values have been reported as being associated with degenerated cartilage, as compared to healthy cartilage [6, 17]. Lammentausta et al. reported T2 relaxation time has further been linked to the mechanical properties of cartilage [18]. In the portion of our study using the 14 recruited volunteers, T2 relaxation times were used as a reference to assess cartilage degeneration. SOS and T2 relaxation times showed strong correlation, and the SOS data observed in our study indicates that these values reflect the degree of degeneration of the cartilage. The cartilage thickness necessary for calculation of the SOS is obtained from a morphological image, against T2-mapping which takes long scan time. It is an advantage of this combined method to use the thickness without complicate image processing against T2-mapping which measure small regions that segmented thin cartilage. However, the SOS has an inadequacy that only local information is provided against T2-mapping which is provided for whole area. Using two modalities to obtain SOS is a demerit, but there is the advantage that the elasticity in vivo cartilage assumed

impossibility is provided.

**Table 6-1**

Summary of reported speed of sound measurements in articular cartilage

Author (year)	Articular cartilage specimen	Speed of sound
Myers et al. (1995)	Human femoral condyle	$1658 \pm 185$ m/s
Suh et al. (2001)	Human femoral condyle	●normal $1735 \pm 35$ m/s
		●PG-depleted $1598 \pm 28$ m/s
Present study using US+MRI	Human femoral condyle	●normal $1684 \pm 68$ m/s (medial)
		$1650 \pm 70$ m/s (lateral)

## 6.5 Conclusions

We demonstrated the accuracy of our proposed method, combining MRI and ultrasound measurements to assess the SOS in cartilage and in human knee cartilage were carried out. SOS observed in our study indicates that these values reflect essential features of the phenomenon same as that of T2 relaxation times, and the accuracy of SOS *in vivo* cartilage was exhibited.



## Chapter 7 Summery

In super-graying society, the quality of life (QOL) decreases by progressive OA remarkably. Therefore diagnostic method to detect early OA is expected to be established to prevent its progression. The development of the early diagnostic method of OA with a noninvasive and quantitative diagnostic method is important and expected. In this research, two new diagnostic methods were proposed using MRI and combination of MRI and ultrasound to quantitatively assess the change of the cartilage in the early stage of OA.

It is known that apparent diffusion coefficient (ADC) shows water content of the cartilage, but change of slight water content was not effective for an evaluation of the cartilage degeneration. ADC was focused on as a parameter of quantitative evaluation for viscoelasticity of the cartilage. As a conclusion, a significant correlation between ADC and viscoelasticity was observed, indicating that ADC can serve as a valuable parameter of non-invasive method of assessing cartilage viscoelasticity.

As a second step, a quantitative evaluation for cartilage elasticity using SOS was proposed and investigated. In this investigation, SOS of the cartilage was demonstrated to be obtained by the combination of MRI and ultrasound and the

measured SOS was shown to correlate with the T2 relaxation times of the corresponding cartilage. And as a result, SOS was demonstrated as a useful indicator for evaluation of the cartilage elasticity.

Two possible biomechanical quantitative evaluation methods were proposed to assess the elasticity of cartilage noninvasively, and their potentials were demonstrated to point out an early change of the cartilage before bony morphological changes appear.

## References

### Chapter 1

1. Armstrong CG, Mow VC: Variations in the mechanical properties of human articular cartilage with age, degeneration, and water content. *J Bone Joint Surg Am* 1982; 64(1): 88-94.
2. Klusmann A, Gebhardt H, Liebers F, von Engelhardt LV, Dávid A, Bouillon B et al. Individual and occupational risk factors for knee osteoarthritis - study protocol of a case control study. *BMC Musculoskelet Disord*. 2008 Feb 26; 9:26
3. Hennerbichler A, Rosenberger R, Arora R, Hennerbichler D. Biochemical, biomechanical and histological properties of osteoarthritic porcine knee cartilage: implications for osteochondral transplantation. *Arch Orthop Trauma Surg* 2008;128(1):61-70.
4. Kuroki H, Nakagawa Y, Mori K, Kobayashi M, Yasura K, Okamoto Y, Suzuki T, Nishitani K, Nakamura T. Ultrasound properties of articular cartilage in the tibio-femoral joint in knee osteoarthritis: relation to clinical assessment (International Cartilage Repair Society grade). *Arthritis Res Ther*. 2008;10(4):R78.

## Chapter 2

1. Mansour JM. Biomechanical Principles Part 1 Chapter 5: 66-78 Biomechanics at the University of Oregon.

<http://www.cartilagehealth.com/images/artcartbiomech.pdf>

2. Goodwin DW, Zhu H, Dunn JF. In vitro MR imaging of hyaline cartilage: correlation with scanning electron microscopy. AJR Am J Roentgenol. 2000; 174(2):405-9.

3. Klusmann A, Gebhardt H, Liebers F, von Engelhardt LV, Dávid A, Bouillon B et al. Individual and occupational risk factors for knee osteoarthritis - study protocol of a case control study. BMC Musculoskelet Disord. 2008; 26; 9:26

4. Adapted from <http://www.spacelan.ne.jp/~tkct/lesion02.htm>

5. Pritzker KP, Gay S, Jimenez SA, Ostergaard K, Pelletier JP, Revell PA et al. Osteoarthritis cartilage histopathology: grading and staging. OsteoArthritis and Cartilage 2006; 14:13-29.

6. Kellgren JH, Lawrence JS. Radiological assessment of osteo-arthritis. Ann Rheum Dis 1957; 16:494-502.

7. Souza RB, Stehling C, Wyman BT, Hellio Le Graverand MP, Li X, Link TM et al. The effects of acute loading on T1rho and T2 relaxation times of tibiofemoral articular cartilage. Osteoarthritis Cartilage 2010; 18(12):1557-63.

8. Ozlem Baysal, Tamer Baysal, Alpay Alkan, Zühal Altay, Saim Yologlu. Comparison of MRI graded cartilage and MRI based volume measurement in knee osteoarthritis. SWISS MED WKLY 2004;134 :283-288.
9. Mlynárik V, Trattnig S, Huber M, Zembsch A, Imhof H. The role of relaxation times in monitoring proteoglycan depletion in articular cartilage. J Magn Reson Imaging 1999; 10(4):497-502.

### Chapter 3

1. Zhu SC, Shi DP, Xuan A. Human patellar cartilage: echo planar diffusion-weighted MR imaging findings at 3.0 T. Clin Imaging. 2012;36(3):199-202.
2. Meder R, de Visser SK, Bowden JC, Bostrom T, Pope JM. Diffusion tensor imaging of articular cartilage as a measure of tissue microstructure. Osteoarthritis Cartilage. 2006; 14(9):875-81.
3. Greene GW, Zappone B, Zhao B, Söderman O, Topgaard D, Rata G, Israelachvili JN. Changes in pore morphology and fluid transport in compressed articular cartilage and the implications for joint lubrication. Biomaterials. 2008;29(33):4455-62.
4. Burstein D, Gray ML, Hartman AL, Gipe R, Foy BD. Diffusion of small solutes in cartilage as measured by nuclear magnetic resonance (NMR) spectroscopy and

imaging. J Orthop Res 1993;11:465-78.

5. Jeffery AK, Blunn GW, Archer CW, Bentley G. Three dimensional collagen architecture in bovine articular cartilage. J Bone Joint Surg (Br) 1991;73:795-801.
6. Bassar PJ, Mattiello J, Le Bihan D. Estimation of the effective self-diffusion tensor from the NMR spin echo. J Magn Reson B 1994;103:247-54.
7. Filidoro L, Dietrich O, Rauch E, Oerther T, Wick M, Reiser MF, et al.  
High-resolution diffusion tensor imaging of human patellar cartilage: feasibility and preliminary findings. Magn Reson Med 2005;53:993-8.

## Chapter 4

1. Armstrong CG, Mow VC: Variations in the mechanical properties of human articular cartilage with age, degeneration, and water content. J Bone Joint Surg Am 1982; 64(1): 88-94.
2. Nieminen MT, Töyräs J, Rieppo J, et al.: Quantitative MR microscopy of enzymatically degraded articular cartilage. Magn Reson Med 2000; 43: 676–681.
3. Lin PC, Reiter DA, Spencer RG: Classification of degraded cartilage through multiparametric MRI analysis. J Magn Reson 2009; 201: 61-67.

4. Wayne JS, Kraft KA, Shields KJ, Yin C, Owen JR, Disler DG: MR imaging of normal and matrix-depleted cartilage: correlation with biomechanical function and biochemical composition. *Radiology* 2003; 228: 493–499.
5. Liess C, Lüsse S, Karger N, Heller M, Glüer CC: Detection of changes in cartilage water content using MRI T2-mapping in vivo. *Osteoarthritis and Cartilage* 2002; 10: 907–913.
6. Nishii T, Kuroda K, Matsuoka Y, Sahara T, Yoshikawa H: Change in knee cartilage T2 in response to mechanical loading. *J Magn Reson Imaging* 2008; 28(1): 175-180.
7. Li X, Ma CB, Link TM, et al.: In vivo T1ρ and T2 mapping of articular cartilage in osteoarthritis of the knee using 3 T MRI. *Osteoarthritis and Cartilage* 2007; 15(7): 789-797.
8. Duvvuri U, Kudchodkar S, Reddy R, Leigh JS: T1ρ relaxation can assess longitudinal proteoglycan loss from articular cartilage in vitro. *Osteoarthritis and Cartilage* 2002; 10: 838–844.
9. Mlynárik V, Trattnig S, Huber M, Zembsch A, Imhof H: The role of relaxation times in monitoring proteoglycan depletion in articular cartilage. *J Magn Reson Imaging* 1999; 10: 497-502.

10. Nissi MJ, Rieppo J, Töyräs J, et al.: Estimation of mechanical properties of articular cartilage with MRI- dGEMRIC, T2 and T1 imaging in different species with variable stages of maturation. *Osteoarthritis and Cartilage* 2007; 15; 1141-1148.
11. Mlynárik V, Sulzbacher I, Bittsanský M, Fuiko R, Trattng S: Investigation of apparent diffusion constant as an indicator of early degenerative disease in articular cartilage. *J Magn Reson Imaging* 2003; 17(4): 440-4.
12. Wheaton A, Casey FL, Gougoutas AJ, et al.: Correlation of T1ρ with fixed charge density in cartilage. *J Magn Reson Imaging* 2004; 20; 519-525.
13. Knauss R, Schiller J, Fleischer G, Kärger J, Arnold K.: Self-Diffusion of Water in Cartilage and Cartilage Components as Studied by Pulsed Field Gradient NMR. *Magn Reson Med* 1999; 41: 285-292.
14. Burstein D, Gray ML, Hartman AL, Gipe R, Foy BD.: Diffusion of small solutes in cartilage as measured by nuclear magnetic resonance (NMR) spectroscopy and imaging. *J Orthop Res.* 1993; 11(4):465-78.
15. Ateshian GA: The role of interstitial fluid pressurization in articular cartilage lubrication. *J Biomech* 2009; 42: 1163-1176.
16. Juras V, Bittsanky M, Majdisova Z, et al.: In vitro determination of biomechanical



- properties of human articular cartilage in osteoarthritis using multi-parametric MRI. *J Magn Reson* 2009; 197(1): 40-7.
17. Fragonas E, Mlynarik V, Jellus V, et al. Correlation between biochemical composition and magnetic resonance appearance of articular cartilage. *Osteoarthritis Cartilage* 1998; 6:24-32.
  18. Goodwin DW, Wadghiri YZ, Zhu H, Vinton CJ, Smith ED, Dunn JF. Macroscopic structure of articular cartilage of the tibial plateau: influence of a characteristic matrix architecture on MRI appearance. *Am J Roentgenol* 2004; 182:311-318.
  19. Smith HE, Mosher TJ, Dardzinski BJ, et al.: Spatial variation in cartilage T2 of the knee. *J Magn Reson Imaging* 2001; 14:50-55.
  20. Wheaton AJ, Borthakur A, Corbo M, Charagundla SR, Reddy R: Method for reduced SAR T1ρ-weighted MRI. *Magn Reson Med* 2004; 51: 1096–102.
  21. Martirosian P, Rommel E, Schick F, Deimling M. Control of susceptibility-related image contrast by spin-lock techniques. *Magn Reson Imaging* 2008; 26:1381–1387.
  22. Vlaardingerbroek MT, den Boer JA: *Magnetic resonance imaging: theory and practice*, 3rd ed. Berlin, Germany: Springer, 2003. p 532
  23. Duvvuri U, Kudchodkar S, Reddy R, Leigh JS: T1ρ relaxation can assess longitudinal proteoglycan loss from articular cartilage in vitro. *Osteoarthritis and*

- Cartilage 2002; 10: 838–844.
24. Witschey WR, Borthakur A, Elliott MA et al.: T1ρ-prepared balanced gradient echo for rapid 3D T1ρ MRI. *J Magn Reson Imaging* 2008; 28(3):744-54.
25. Scheffler K: On the transient phase of balanced SSFP sequences. *Magn Reson Med* 2003; 49: 781–3.
26. Nugent AC, Johnson GA: T1ρ imaging using magnetization-prepared projection encoding (MaPPE). *Magn Reson Med* 2000; 43(3):421-8.
27. Hargreaves BA, Shreyas S. Vasanawala, John M. Pauly, and Dwight G. Nishimura. Characterization and Reduction of the Transient Response in Steady-State MR Imaging. *Magn Reson Med*; 2001: 46:149–158.
28. Niinimäki J, Korkiakoski A, Ojala O, Karppinen J, Ruohonen J, Haapea M et al.: Association between visual degeneration of intervertebral discs and the apparent diffusion coefficient. *Magn Reson Imaging* 2009; 27: (5): 641-647.
29. Sakai N, Hagihara Y, Furusawa T, Hosoda N, Sawae Y, Murakami T: Analysis of biphasic lubrication of articular cartilage loaded by cylindrical indenter. *Tribology International* In Press, Corrected Proof 2011; 1-12.
30. Park S, Krishnan R, Nicoll SB, Ateshian GA: Cartilage interstitial fluid load support in unconfined compression. *J Biomech* 2003; 36: 1785-1796.

31. Li LP, Korhonen RK, Iivarinen J, Jurvelin JS, Herzog W: Fluid pressure driven fibril reinforcement in creep and relaxation tests of articular cartilage. *Med Eng Phys* 2008; 30(2): 182-189.
32. Li LP, Herzog W, Korhonen RK, Jurvelin JS: The role of viscoelasticity of collagen fibers in articular cartilage: axial tension versus compression. *Med Eng Phys* 2005; 27(1): 51-57.
33. Lai WM, Mow VC: Biphasic indentation of articular cartilage-I. Theoretical analysis. *J Biomech* 1987; 20: 703-714.
34. Greene GW, Zappone B, Zhao B, et al.: Changes in pore morphology and fluid transport in compressed articular cartilage and the implications for joint lubrication. *Biomaterials* 2008; 29(33): 4455-4462.
35. Ohmori Y, Tsukamoto Y: A study on the volume and chemistry of fluid exuded from normal articular cartilage under pressure. *Kitasato Med* 1991; 21: 288-297.
36. Timonen MA, Töyräs J, Aula AS, Karjalainen JP, Riekkinen O, Jurvelin JS: Technical and practical improvements in arthroscopic indentation technique for diagnostics of articular cartilage softening. *J Med Eng Technol* 2011; 35(1): 40-6.

## Chapter 5

1. Kaleva E, Saarakkala S, Töyräs J, Nieminen HJ, Jurvelin JS. In-vitro comparison of time-domain, frequency-domain and wavelet ultrasound parameters in diagnostics of cartilage degeneration. *Ultrasound Med Biol* 2008; 34:155-9.
2. Wang SZ, Huang YP, Saarakkala S, Zheng YP. Quantitative assessment of articular cartilage with morphologic, acoustic and mechanical properties obtained using high-frequency ultrasound. *Ultrasound Med Biol* 2010;36:512-27.
3. Chiang EH, Adler RS, Meyer CR, Rubin JM, Dedrick DK, Laing TJ. Quantitative assessment of surface roughness using backscattered ultrasound: The effects of finite surface curvature. *Ultrasound Med Biol* 1994;20:123-35.
4. Myers SL, Dines K, Brandt DA, Brandt KD, Albrecht ME. Experimental assessment by high frequency ultrasound of articular cartilage thickness and osteoarthritic changes. *J Rheumatol* 1995;22:109-16.
5. Joiner GA, Bogoch ER, Pritzker KP, Buschmann MD, Chevrier A, Foster FS. High frequency acoustic parameters of human and bovine articular cartilage following experimentally-induced matrix degradation. *Ultrason Imaging* 2001;23:106-16.

6. Aula AS, Töyräs J, Tiitu V, Jurvelin JS. Simultaneous ultrasound measurement of articular cartilage and subchondral bone. *Osteoarthritis Cartilage* 2010; 18: 1570-1576.
7. Jurvelin JS, Räsänen T, Kolmonen P, Lyyra T. Comparison of optical, needle probe and ultrasonic techniques for the measurement of articular cartilage thickness. *J Biomech* 1995;28:231-5.
8. Töyräs J, Laasanen MS, Saarakkala S, Lammi MJ, Rieppo J, Kurkijärvi J, Lappalainen R, Jurvelin JS. Speed of sound in normal and degenerated bovine articular cartilage. *Ultrasound Med Biol* 2003;29:447-54.
9. Ohashi S, Ohnishi I, Matsumoto T, Bessho M, Matsuyama J, Tobita K, Kaneko M, Nakamura K. Evaluation of the accuracy of articular cartilage thickness measurement by B-mode ultrasonography with conventional imaging and real time spatial compound ultrasonography imaging. *Ultrasound Med Biol* 2012; 38:324-34.
10. Lee JH, Kim SH, Kang BJ, Choi JJ, Jeong SH, Yim HW, Song BJ. Role and clinical usefulness of elastography in small breast masses. *Acad Radiol* 2011;18(1):74-80.

11. Park DW, Richards MS, Rubin JM, Hamilton J, Kruger GH, Weitzel WF. Arterial elasticity imaging: comparison of finite-element analysis models with high-resolution ultrasound speckle tracking. *Cardiovasc Ultrasound*. 2010;18:8-22.
12. Saarakkala S, Korhonen RK, Laasanen MS, Töyräs J, Rieppo J, Jurvelin JS. Mechano-acoustic determination of Young's modulus of articular cartilage. *Biorheology* 2004;41:167-79.
13. Cannon LM, Fagan AJ, Browne JE. Novel tissue mimicking materials for high frequency breast ultrasound phantoms. *Ultrasound Med Biol*. 2011; 37(1):122-35.
14. Saarakkala S, Laasanen MS, Jurvelin JS, Törrönen K, Lammi MJ, Lappalainen R, Töyräs J. Ultrasound indentation of normal and spontaneously degenerated bovine articular cartilage. *Osteoarthritis Cartilage* 2003; 11(9):697-705.
15. Patil SG, Zheng YP, Chen X: Site dependence of thickness and speed of sound in articular cartilage of bovine patella. *Ultrasound Med Biol* 2010; 36(8):1345-52.
16. Eckstein F, Sittek H, Milz S, Schulte E, Kiefer B, Reiser M, Putz R. The potential of magnetic resonance imaging (MRI) for quantifying articular cartilage thickness-a methodological study. *Clin Biomech (Bristol, Avon)* 1995; 10(8):434-40.
17. Eckstein F, Adam C, Sittek H, Becker C, Milz S, Schulte E, Reiser M, Putz R.

Non-invasive determination of cartilage thickness throughout joint surfaces using magnetic resonance imaging. J Biomech 1997; 30:285-9.

## Chapter 6

1. Suh JK, Youn I, Fu FH. An in situ calibration of an ultrasound transducer: A potential application for an ultrasonic indentation test of articular cartilage. J Biomech 2001; 34:1347-53.
2. Lee SC, Coan BS, Buxsein ML. Tibial ultrasound velocity measured in situ predicts the material. Bone 1997; 21(1):119-25.
3. Walker JM, Myers AM, Schluchter MD et al. Nondestructive evaluation of hydrogel mechanical properties using ultrasound. Ann Biomed Eng 2011; 39(10): 2521-2530.
4. Kiviranta P, Lammentausta E, Töyräs J et al. Differences in acoustic properties of intact and degenerated human patellar cartilage during compression. Ultrasound Med Biol 2009; 35(8):1367-75.
5. Ohashi S, Ohnishi I, Matsumoto T et al. Evaluation of the accuracy of articular cartilage thickness measurement by B-mode ultrasonography with conventional imaging and real time spatial compound ultrasonography imaging. Ultrasound Med

Biol 2012; 38:324-34.

6. Li X, Benjamin Ma C, Link TM et al. In vivo T1ρ and T2 mapping of articular cartilage in osteoarthritis of the knee using 3 T MRI. *Osteoarthritis Cartilage*. 2007; 15: 789-97.
7. Keenan KE, Besier TF, Pauly JM et al. Prediction of glycosaminoglycan content in human cartilage by age, T1ρ and T2 MRI. *Osteoarthritis and Cartilage* 2011; 19: 171-179.
8. Akhtar S, Poh CL, Kitney RI. An MRI derived articular cartilage visualization framework. *Osteoarthritis Cartilage* 2007; 15(9):1070-85.
9. Nakano S, Yoshida M, Fujii K et al. Fusion of MRI and sonography image for breast cancer evaluation using real-time virtual sonography with magnetic navigation: first experience. *Jpn J Clin Oncol* 2009; 39(9):552-9.
10. Cohen ZA, McCarthy DM, Kwak SD et al. Knee cartilage topography, thickness, and contact areas from MRI: in-vitro calibration and in vivo measurements. *Osteoarthritis Cartilage* 1999; 7(1):95-109.
11. Stammberger T, Hohe J, Englmeier KH, Reiser M, Eckstein F. Elastic registration of 3D cartilage surfaces from MR image data for detecting local changes in cartilage thickness. *Magn Reson Med* 2000; 44(4):592-601.



12. Eckstein F, Sittek H, Milz S et al. The potential of magnetic resonance imaging (MRI) for quantifying articular cartilage thickness-a methodological study. Clin Biomech (Bristol, Avon) 1995; 10(8):434-40.
13. Eckstein F, Adam C, Sittek H et al. Non-invasive determination of cartilage thickness throughout joint surfaces using magnetic resonance imaging. J Biomech 1997; 30:285-9.
14. Myers SL, Dines K, Brandt DA, Brandt KD, Albrecht ME: Experimental assessment by high frequency ultrasound of articular cartilage thickness and osteoarthritic changes. J Rheumatol. 1995; 22:109–116.
15. Joiner GA, Bogoch ER, Pritzker KP, Buschmann MD, Chevrier A, Foster FS: High frequency acoustic parameters of human and bovine articular cartilage following experimentally-induced matrix degradation. Ultrason Imaging. 2001; 23:106–116.
16. Nieminen MT, Nissi MJ, Mattila L, Kiviranta I. Evaluation of Chondral Repair Using Quantitative MRI. J Magn Reson Imaging. 2012;36: 1287–1299.
17. Bolbos RI, Zuo J, Banerjee S et al. Relationship between trabecular bone structure and articular cartilage morphology and relaxation times in early OA of the knee joint. Osteoarthritis Cartilage. 2008;16: 1150-1159.
18. Lammentausta E, Kiviranta P, Nissi MJ, et al. T2 relaxation time and delayed

gadolinium-enhanced MRI of cartilage (dGEMRIC) of human patellar cartilage at 1.5 T and 9.4 T: relationships with tissue mechanical properties. J Orthop Res 2006;24:366–374.

## Acknowledgment

本研究のご指導をいただきました新津守先生、福士政広先生、古川顕先生、千葉帝京大学病院の渡辺淳也先生、産業技術総合研究所の新田尚隆先生に感謝いたします。

新津守先生は、全く研究をしたこともなく、業績も全くない私を研究室に入れてくださり、新しい世界のスタートに立たせてもらいました。要所々で適切なアドバイスをいただき、だんだんと、辛さよりも研究が楽しいと思うまでに成長させてくださいました。修士では RSNA に連れて行ってくださり、世界レベルの高さに圧倒されましたが、刺激となり奮起して博士課程では目標としていた ISMRM で発表をすることができました。1 年目で埼玉医大に移動されることになりましたが、最後まで見届けていただきありがとうございました。

新津先生が去られ、不安でいっぱいでしたが、福士政広先生が一時的に指導教官を引き受けてくださり、ホッとしました。MRI の使用に関しても、実験が遂行できるように配慮し、常に見守ってくださり本当に感謝の気持ちでいっぱいです。ゼミでは、先生からいろいろなお話を伺い、不安も徐々になくなりました。福士研には学部生、院生とも暖かく受け入れていただき、ありがとうございました。同世代の院生もおられ、仲間ができて色々な話をする機会ができ、楽しく過ごすことができました。

古川顕先生には、着任早々指導教官を引き受けていただき感謝しています。一番要の論文指導をお願いし、専門外の分野にもかかわらず、一つ一つ丁寧に時間をかけて指導してくださり、投稿論文まで見ていただき本当にありがとうございました。

千葉帝京大学病院整形外科の渡辺淳也先生には、お忙しい中、すべての投稿論文の指導を根気よく長期間にわたって、ご指導いただき本当に感謝しています。整形外科と放射線科の両方の専門医であり、気さくなお人柄に加え関節軟骨では、高名で世界

トップレベルの渡辺淳也先生のご指導を受けることができ、幸運に恵まれました。渡辺先生のご指導のおかげで投稿論文がアクセプトされました。ありがとうございました。

3年にわたり本研究の研究指導をしてくださった、産業技術総合研究所の新田尚隆先生には、超音波、力学試験、MRIと多岐にわたる指導をしていただきました。初めて産総研でプレゼンをさせていただいき、研究指導をお願いした時は、超音波の難しさも、力学試験の方法も知らない状態でしたが、快く引き受けてくださり、新津守先生が去られるという不測の事態の中でも、研究を続行させていただき、感謝しています。何度も失敗し、なかなか結果が出ませんでしたが、粘り強く指導をしていただき、3年越しでやっと結果を出すことができ、感謝しています。論文指導は負担になるので、新津先生からお願いしないようにと釘を刺されていましたが、新田尚隆先生には、投稿論文の指導もさせていただきました。なかなかうまく論文が書けず、時間ばかりが過ぎてしまいましたが、新田尚隆先生の根気強いご指導に助けられました。超音波学会での学会発表もご指導いただきありがとうございました。

ブタの実験では、入手に苦勞し途方に暮れていたところを、全農飼料畜産中央研究所の落合成年副所長に助けていただき、無理なお願いをして特別に処理をしていただいたブタ膝を提供していただきました。実際に、屠畜場を見学させていただき、貴重なお話を伺い、また、ボランティアとして被験者も引き受けてくださいました。本研究の柱である、ブタ軟骨標本の提供を受けることができなかつたら、ここまで、たどり着くことはできませんでした。落合さんのご協力には本当に感謝しています。ありがとうございました。

新津研をはじめ、八木研、妹尾研、篠原研、福土研の学部生、院生の皆様、国立スポーツ科学センターの本田亜紀子さんをはじめ研究者、STAFFの皆様、被験者として協力していただき、本当にありがとうございました。

皆様のご協力のおかげをもちまして、博士論文を書くことができました。本当にありがとうございました。

ご指導・ご協力くださったすべての方に感謝の意を表します。

